Decarbonising the iron and steel industries: Production of carbon-negative direct reduced iron by using biosyngas

(article starts on next page)

Decarbonising the iron and steel industries: Production of carbon-negative direct reduced iron by using biosyngas

Ilman Nuran Zaini [a,*], Anissa Nurdiawati [b], Joel Gustavsson [c], Wenjing Wei [a,c], Henrik Thunman [d], Rutger Gyllenram [c], Peter Samuelsson [a], Weihong Yang [a]

[a] *Department of Materials Science and Engineering, KTH Royal Institute of Technology, Sweden*
[b] *Department of Industrial Economics and Management, KTH Royal Institute of Technology, Sweden*
[c] *Kobolde & Partners AB, Stockholm, Sweden*
[d] *Department of Space, Earth, and Environment, Division of Energy Technology, Chalmers University of Technology, 412 96 Göteborg, Sweden*

ARTICLE INFO

ABSTRACT

Bioenergy with carbon capture and storage (CCS) in iron and steel production offers significant potential for CO_2 emission reduction and may even result in carbon-negative steel. With a strong ambition to reach net-zero emissions, some countries, such as Sweden, have recently proposed measures to incentivise bioenergy with CCS (BECCS), which opens a window of opportunities to enable the production of carbon-negative steel. One of the main potential applications of this route is to decarbonise the iron reduction processes that account for 85 % of the total CO_2 emission in the iron and steel plants. In this study, gasification is proposed to convert biomass into biosyngas to reduce iron ore directly. Different cases of integrating the biomass gasifier, Direct Reduced Iron (DRI) shaft furnace, and CCS are evaluated through process simulation work. Based on the result of the work, the proposed biosyngas DRI route has comparable energy demand compared to other DRI routes, such as the well-established coal gasification and natural gas DRI route. The proposed process can also capture 0.65–1.13 t of CO_2 per t DRI depending on the integration scenarios, which indicates a promising route to achieving carbon-negative steel production.

1. Introduction

The iron and steel industry is a major resource and energy-intensive industry. It is the largest industrial emitter of CO_2 among heavy industries, accounting for approximately 7 % of global energy-related emissions and 7–9 % of global anthropogenic CO_2 emissions [1]. Primary steel production (i.e., steel made from iron ore, unlike secondary steelmaking made from recycled scrap) is the major source of those emissions due to its reliance on fossil carbon in blast furnaces (BFs). The BF process currently dominates the ironmaking technologies and is responsible for 80 % of the total CO_2 emissions from primary iron and steel production [2]. Fossil-free ironmaking, therefore, has the biggest leverage for achieving deep emission cuts from this sector and reaching a net zero target by 2050 following the Paris Agreement. Correspondingly, the transition from the conventional BF process to scrap-based steel production through electric arc furnaces (EAFs) has been considered the main route for decarbonising the steel industries [3]. However, the transition to scrap-based steelmaking will potentially cause a lack of high-quality scrap, leading to the increased demand for fossil-free DRI (also called sponge iron) to replace the high-quality scrap. As a result, accelerating the production of fossil-free DRI is a key part of the transition to a sustainable steelmaking route.

Biomass-based DRI routes can be attractive, particularly for countries with sufficient and sustainable domestic resources. Substantial attention has been devoted to the increase of biomass use in the iron and steel industry, considering its renewability, availability and versatility [4,5]. Combining biomass use with carbon capture and storage in the so-called BECCS is gaining more interest as an effective strategy for achieving net-zero emissions or even creating negative emissions. Countries with ambitious climate targets, like Sweden, have made an effort to incentivise BECCS [6], which opens the window of opportunity for BECCS implementation in the iron and steel sector. In addition, the biomass utilisation route could offer an alternative complement pathway to the H_2-based DRI route. H_2-based DRI production pathway offers a huge potential for fossil-free DRI production thanks to green H_2 and renewable electricity utilisation. This pathway has gained

significant momentum and is currently the main decarbonisation strategy considered by the EU steel industry [3]. Despite the potential, deploying H$_2$-based DRI to decarbonise steelmaking needs a substantial amount of renewable electricity, adequate grid and H$_2$ infrastructure, and cost-effective H$_2$ that needs to be addressed by a range of measures [7].

Comprehensive reviews have been conducted to explore opportunities and challenges of potential biomass applications in the iron and steel industry; for examples see [8–10]. Much attention has been placed on using biochar to replace coal and coke in the BF or reducing agents in a DRI process. For instance, Suopajärvi et al. [11,12] develop a technical concept and economic analysis of biochar utilisation for a Nordic BF. Han et al. [13] evaluate biomass utilisation (bamboo char, charcoal and straw fibre) in the rotary hearth furnace process to produce DRI. Suman and Yadav [14] also performed a comparative study on the direct reduction of iron ore pellets using different biochar reductants. Those studies demonstrated that biochars could be used as a reducing agent for replacing coking coal in iron- and steelmaking. In contrast to biochar-based iron making, there are fewer studies on biomass-derived gas for DRI production. The use of biomass-derived gas is especially an interesting option, considering that the most common technologies used for the current DRI production are gas-based such as MIDREX and HYL-III. Approximately 60 % of the global DRI are currently produced by MIDREX plants [15]. In these technologies, syngas (synthetic gas) containing mainly of H$_2$ and CO are produced from natural gas through a reforming process and used as a reducing agent to reduce iron ore into DRI.

Gasification is a key technology for producing biomass-derived syngas (biosyngas) and has been studied widely in the literature, especially regarding process configuration [16]. Biomass gasification is a mature technology as the commercial installations of biomass gasification plants over the last decades suggest a high technology readiness level (TRL) for biomass gasification technology, on the order of 7–9 [17]. Considering the maturity of both gasification and DRI technologies, the integration of the two processes can be considered a "low-hanging fruit" that provides the opportunity to facilitate biomass use within the iron and steel industry. When combined with carbon capture, the integration would also enable the production of pure CO$_2$ ready for transport/use and create a substantive opportunity to produce carbon-negative steel. Additionally, biosyngas as a reducing agent is beneficial due to the ability to adapt to existing gas-based DRI shaft furnaces owing to the fuel similarities with the conventional syngas from natural gas. The DRI produced from biosyngas could also have similar characteristics to fossil-based DRI. Correspondingly, the need for reconfiguring the current well-established DRI/EAF steelmaking route can be minimised when using biosyngas for producing the DRI.

Despite the potential, the integration of biomass gasification, DRI processes, and CCS has not been extensively investigated. Previous studies have proposed the application of biomass gasification for steel plants; nevertheless, they mainly investigated the production of biosyngas and bio-SNG (synthetic natural gas) for heating the industrial furnace in steel plants [18–20]. Furthermore, few other studies have previously focused solely on either biomass-based DRI or CCS for iron and steel production without integration. For instance, Grip et al. [21] investigated the production of DRI using gasified biomass as the reducing agent. They evaluated the supply chain aspects, yet full process integration between different modules was not presented, and the possibility of integration with the CCS unit was not evaluated in depth. Our previous study has evaluated the possibility of using biosyngas for DRI production coupled with CCS [22]. Nevertheless, in this study, a chemical looping gasification of biomass (TRLs 5–6 [23]) combined with an electrolyser is considered for producing biosyngas instead of other mature gasification technologies with higher TRLs.

This paper's overall objective is to propose a novel integration system of biosyngas-based DRI production coupled with CCS. Fluidised bed gasifier technologies with TRLs of 9 are considered in this study. A process simulation model is developed to evaluate the proposed

system's energy efficiency and flexibility in the choice of energy source. Furthermore, different integration scenarios are also developed to evaluate the application of different syngas cleaning technologies, an integrated biomass dryer, and an additional H$_2$ electrolyser.

2. Methods

2.1. Description of the system

The proposed system consists of a biomass dryer, a gasifier, a tar reforming/removal process, a gas heater, a DRI shaft furnace (similar to the MIDREX furnace), and a CO$_2$ removal process. Fig. 1 presents the schematic diagram of the proposed biosyngas DRI production system. The wet biomass is first subjected to a drying process to reduce its moisture content. The dried biomass is then fed to the gasification process, in which the biomass is converted into raw syngas, unreacted char, and ash. Atmospheric fluidised bed biomass gasifiers are adapted for the proposed system, specifically due to the maturity and the scalability of these technologies, which already reach hundreds of MW capacity.

This study evaluates two gasifier technologies: the steam/oxygen-blown Circulating Fluidised Bed (CFB) gasifier and the steam-blown Dual Fluidised Bed (DFB) gasifier. CFB gasifiers consist of a riser, in which biomass undergoes moisture evaporation, pyrolysis, and char gasification. The CFB gasifiers are an extension of the bubbling bed concept with additional high-temperature cyclones or other separators that capture and recycle solids (char and bed material) to extend the solid residence time [24]. The captured solids from the product gas are recycled back to the bottom of the riser through an air-driven loop seal. In the case of steam/oxygen-blown CFB, the heat for endothermic reduction reactions is provided by injecting O$_2$ to allow exothermic oxidation reactions. Meanwhile, steam is added to fluidise the fuel and bed material. The capacity of current existing CFB commercial plants can be up to 160 MW, larger than the existing DFB gasifiers that are normally smaller than 25 MW [25]. In addition, due to the simpler reactor configuration, CFB gasifiers may demand a lower capital cost than DFB gasifiers [25].

In contrast to the CFB gasifiers, DFB gasifiers are commonly known as indirect gasifiers due to the heat for gasification is provided by a circulating hot bed material. The gasification process involves two connected fluidised bed reactors: a gasifier and a combustor. Biomass is fed into the gasifier riser and then fluidised by the steam and producer gas together with the bed material. The producer gas will then be separated from the solids. After that, the solids, which include bed material and char, are fed to the combustor. Then the char is combusted by air to heat the bed material at a temperature higher than the gasifier. The hot bed material is then returned to the gasifier to provide the heat needed for the gasification. As the major part of the combustion reaction occurs outside the gasifier, DFB gasifiers allow the production of syngas with a lower CO$_2$ and a higher H$_2$ concentration than CFB gasifiers. Another benefit of the DFB gasifier is the possibility of recovering biochar from the gasifier by using a carbon stripper [26]. The recovered biochar can be used for the subsequent steelmaking processes; thus, it can also potentially decarbonise the steelmaking processes by replacing the conventional fossil-based coke and carbonaceous materials.

The raw syngas from the gasifier typically contains a significant amount of tar compounds, mainly benzene, toluene, xylene, and heavy tar compounds (e.g., naphthalene). Hence, a tar removal process is required to prevent potential problems caused by the condensation of tar in the subsequent processes. This study evaluated two options: tar removal by wet scrubber and tar reforming process. The wet scrubber methods have the benefits of low energy demand and the ability to recover the valuable BTX fraction (i.e., benzene, toluene, and xylene) as bio-chemical products that can be sold to the market; thus, it can be used for maximum value creation in the bioeconomy. Additional solvents are needed for the wet scrubber, which can be extracted from the produced
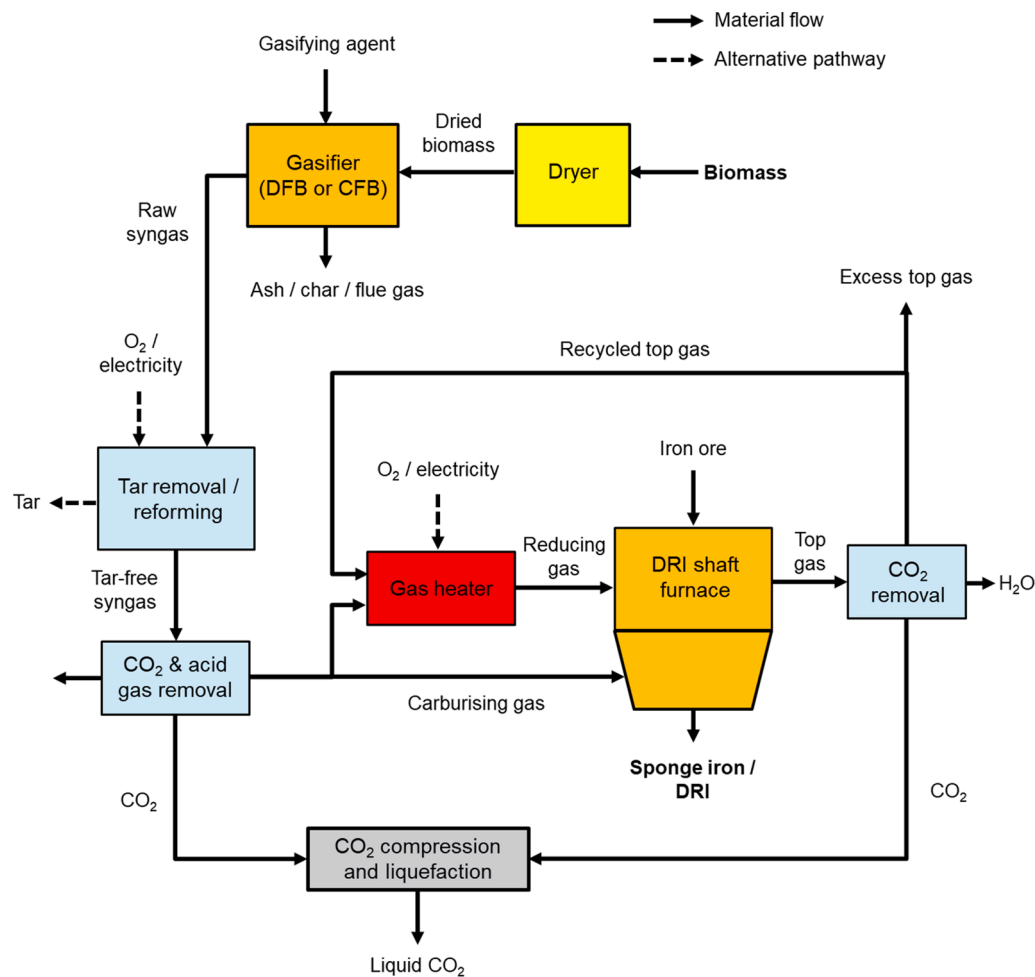
Fig. 1. The general overview of the proposed biosyngas DRI production system.

tars or externally provided. On the other hand, tar reforming reactions are endothermic and favour high operating temperatures (>800 °C); hence, the process is energy intensive. However, reforming processes can maximise biomass conversion to high-quality reducing gas, as it converts the tar into H_2 and CO. Thus, the produced raw syngas from gasifiers can be either valorised for maximum production of chemical byproduct or DRI, depending on the value of those products.

After the tar cleaning processes, the tar-free syngas is cooled and upgraded to improve its quality as a reducing gas in terms of the reduction potential (RP). RP is an important parameter for the reducing gas, which can be defined as the molar ratio of $(H_2 + CO)/(H_2O + CO_2)$. A lower RP value will reduce the efficiency of the DRI processes [22]. Existing gas-based DRI shaft furnaces are typically operated with RP values higher than 9 [27]. The syngas produced from biomass gasification normally contains a high concentration of CO_2 and H_2O due to the high oxygen content in the biomass and the use of steam as a fluidisation agent. Hence, a CO_2 removal step is needed in the production system to increase the RP value of the reducing gas derived from biosyngas. In this step, H_2O and acid gases (e.g., H_2S) are removed together with CO_2. This study considers an amine-based CO_2 removal using a 30 wt% aqueous monoethanolamine (MEA) solution because of its maturity and proven commercial technology [46]. In this removal process, the MEA absorbent is regenerated through a stripper equipped with a reboiler unit. The reboiler unit accounts for the main energy demand of the CO_2 removal process [46].

After that, the reducing gas is preheated and injected into the DRI shaft furnace. The reactions that occur in the shaft furnace convert the iron ore into hot sponge iron while producing CO_2 and H_2O that go out

from the reactor as a top gas together with the unreacted H_2 and CO. Thereafter, another CO_2 removal process is added to elevate the RP value of the top gas; thus, it can be recycled back to the shaft furnace as a reducing gas. In this proposed system, the separated CO_2 are compressed and liquefied. The liquefied biogenic CO_2 can then be transported and stored for carbon-negative emission or sold to the market for chemical and biofuel production.

This study considers two potential feedstocks from primary woody biomass residues of forestry industries, namely wood pellets and the "tops and branches" fraction of the logging residue. Wood pellets are typically produced from sawmill residues and have a benefit of a well-established market. On the other hand, logging residues have the benefit of relatively lower cost and a significant amount of untapped potential resources, especially in forest-rich countries such as Sweden. It is estimated that the total growth in Swedish productive forest is approximately 450 TWh/year [28], of which there are 40–55 TWh of untapped potential in the form of tops and branches left in the forest after harvesting [28,29]. This value represents a significant resource considering that the current consumption of coal/coke in the Swedish iron and steelmaking plants is approximately 14 TWh [28].

The aforementioned biosyngas DRI production system is modelled and evaluated using the Aspen Plus V12 software package [30]. The simulations assumed that the processes are operated at steady-state conditions and that gases are treated as ideal gases. Different integration scenarios between different processes are proposed, as presented in the subsequent section below.

2.2. Integration scenarios

This study proposes several integration scenarios based on the different types of gasifiers and heat sources for tar reformers. Table 1 summarises the details of those integration scenarios. The scenarios consist of two main categories, which are steam DFB-based scenarios and steam/oxygen CFB-based scenarios. Different integration varieties are proposed for each main category based on the application of an air separation unit (ASU), electrolyser, or electrified tar reformer. For instance, the steam DFB scenarios consist of DFB-Scrubber, DFB-ASU-O_2, DFB-Electrolyser-O_2, and DFB-Electroreformer. In DFB-Scrubber case, a wet scrubber process is used to remove BTX and heavy tars from syngas, where BTX is recovered as a product and the heavy tar fraction is used in the combustor section of the DFB gasifier. DFB-ASU-O_2 corresponds to the case in which an ASU is used to supply O_2 for the autothermal tar reformer and gas heater. Meanwhile, in DFB-Electrolyser-O_2 scenario, an electrolyser is used to provide the O_2 instead of an ASU. In this case, the produced H_2 from the electrolyser is used as an additional reducing gas. Lastly, DFB-Electroreformer represents a case where the tar reformer and gas heater are fully electrified; thus, no ASU or electrolyser is needed. For the scenarios mentioned above, biomass is assumed to have a moisture content (MC) of 8 wt%, which corresponds to the typical MC value of woody biomass pellets [31]. Thus, a biomass dryer is not used for these scenarios. The schematic diagram of those steam DFB integration scenarios without a biomass dyer is shown in Fig. 2. On the other hand, the steam/oxygen CFB scenarios consist of CFB-ASU-O_2, CFB-Electrolyser-O_2, and CFB-Electroreformer cases which have the same concept to that of DFB-ASU-O_2, DFB-Electrolyser-O_2, and DFB-Electroreformer, respectively. Fig. 3 presents the schematic diagram of the CFB integration scenarios without a biomass dryer.

Further integration scenarios are proposed to handle a wet biomass feedstock with an MC of 40 wt%. This level of MC is selected to represent the typical MC of logging residues from forestry industries in the form of wood chips. These scenarios are developed based on the low-electricity scenarios (i.e., DFB-ASU-O_2 and CFB-ASU-O_2 cases) considering the role of the proposed biosyngas DRI system to provide an alternative fossil-free DRI route other than the electrification pathways, such as H_2-based DRI. These integration scenarios are named DFB-ASU-O_2+dryer and CFB-ASU-O_2+dryer. The schematic diagrams of those scenarios with dryer addition are shown in Fig. 4 and Fig. 5, respectively. In this study, the wet biomass feedstock is assumed to be received in chipped form; thus, the biomass handling plant prior to the dryer is not in the scope of the study.

2.3. Process modelling

2.3.1. Feedstock compositions

The fuel properties of the biomass (on a dry basis) used in this study are shown in Table 2, which is obtained from the composition of wood pellets measured by Alamia et al. [31]. The fuel properties are used for representing both the wood pellets and the logging residues biomass. This assumption is used by considering that the ultimate composition of those woody biomass materials is normally not significantly varied, as seen in Table S.1 in the supplementary material. Thus, in the process simulation, those two feedstocks only differ in moisture content. The calorific value of feedstock and products are presented on a lower heating value (LHV) basis. Meanwhile, Table 3 shows the composition of iron ore used in this study, which represents a typical composition of the DR-grade pellets produced by the Swedish iron ore supplier [32]. In this process simulation study, the gangue fraction is modelled as inert SiO_2 for simplification.
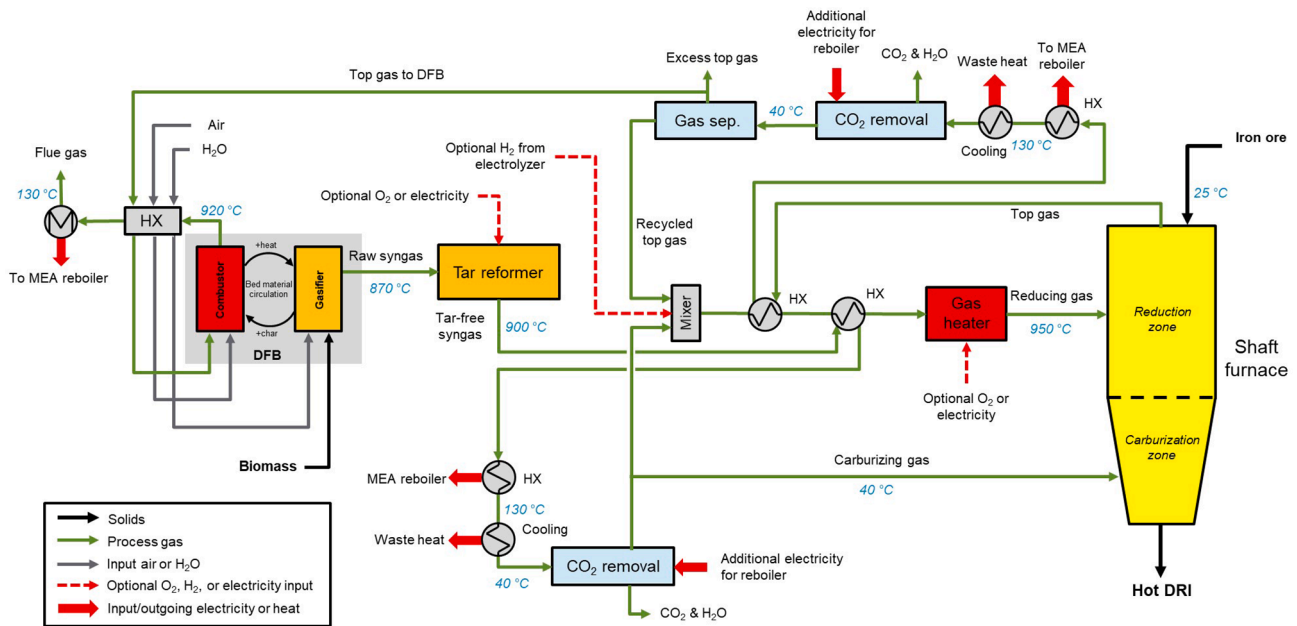
2.3.2. Biomass drying

The biomass dryer is assumed to be a steam belt dryer heated by using excess top gas from the DRI furnace. This drying method is selected as it allows the heated moisture content to be used as fluidisation steam for the gasifier [33]. In this concept, the excess top gas is combusted to generate superheated steam that will be injected into the drying chamber. After that, the energy needed to evaporate the moisture content is supplied through direct contact between the wet biomass particle and the injected superheated steam. The steam that has passed through the bed is then separated to remove the flow of the evaporated moisture and maintain the mass balance of the circulated steam within the dryer. This circulated steam will be heated with the top gas combustion and injected back into the drying chamber.

In the dryer model, an RStoic-block is used to represent the combustion of the top gas fuel. The detailed functions of the reactor blocks used in the simulation software are described in Table 4. Two Heater-blocks are used to model the circulated superheated steam, which transfers the heat from the hot flue gas to the wet biomass stream. The evaporated moisture is then separated from the dried biomass using a Sep-block. The final temperature of the dryer outlet is assumed at 130 °C [33], while the final temperature of the flue gas is set at 140 °C. Fig. 6 presents the schematic diagram of the biomass dryer model.

2.3.3. Gasifier model

2.3.3.1. Steam/oxygen-blown CFB.
An actual gasification process is typically a non-equilibrium process as the carbon in biomass is not fully

Table 1
Description of the investigated integration scenarios.

Integration scenarios	Feedstock	Feedstock moisture content (wt.%)	Biomass dryer	Type of gasifier	Tar elimination	O_2 supplier	Gas heater
DFB-Scrubber	Biomass pellets	8	No	Steam DFB	Wet scrubber	ASU	Partial oxidation
DFB-ASU-O_2	Biomass pellets	8	No	Steam DFB	Autothermal tar reformer	ASU	Partial oxidation
DFB-Electrolyser-O_2	Biomass pellets	8	No	Steam DFB	Autothermal tar reformer	Electrolyser	Partial oxidation
DFB-Electroreformer	Biomass pellets	8	No	Steam DFB	Electrified tar reformer	Not required	Electrified gas heater
DFB-ASU-O_2+dryer	Tops and branches	40	Yes	Steam DFB	Autothermal tar reformer	ASU	Partial oxidation
CFB-ASU-O_2	Biomass pellets	8	No	Steam/oxygen CFB	Autothermal tar reformer	ASU	Partial oxidation
CFB-Electrolyser-O_2	Biomass pellets	8	No	Steam/oxygen CFB	Autothermal tar reformer	Electrolyser	Partial oxidation
CFB-Electroreformer	Biomass pellets	8	No	Steam/oxygen CFB	Electrified tar reformer	ASU[a]	Electrified gas heater
CFB-ASU-O_2+dryer	Tops and branches	40	Yes	Steam/oxygen CFB	Autothermal tar reformer	ASU	Partial oxidation

[a] ASU is used for supplying oxygen to the CFB gasifier.

Fig. 2. Schematic diagram of the process integration based on steam-blown DFB gasifier with a tar reformer and without biomass dryer (i.e., DFB-ASU-O$_2$, DFB-Electrolyser-O$_2$, or DFB-Electroreformer scenarios).
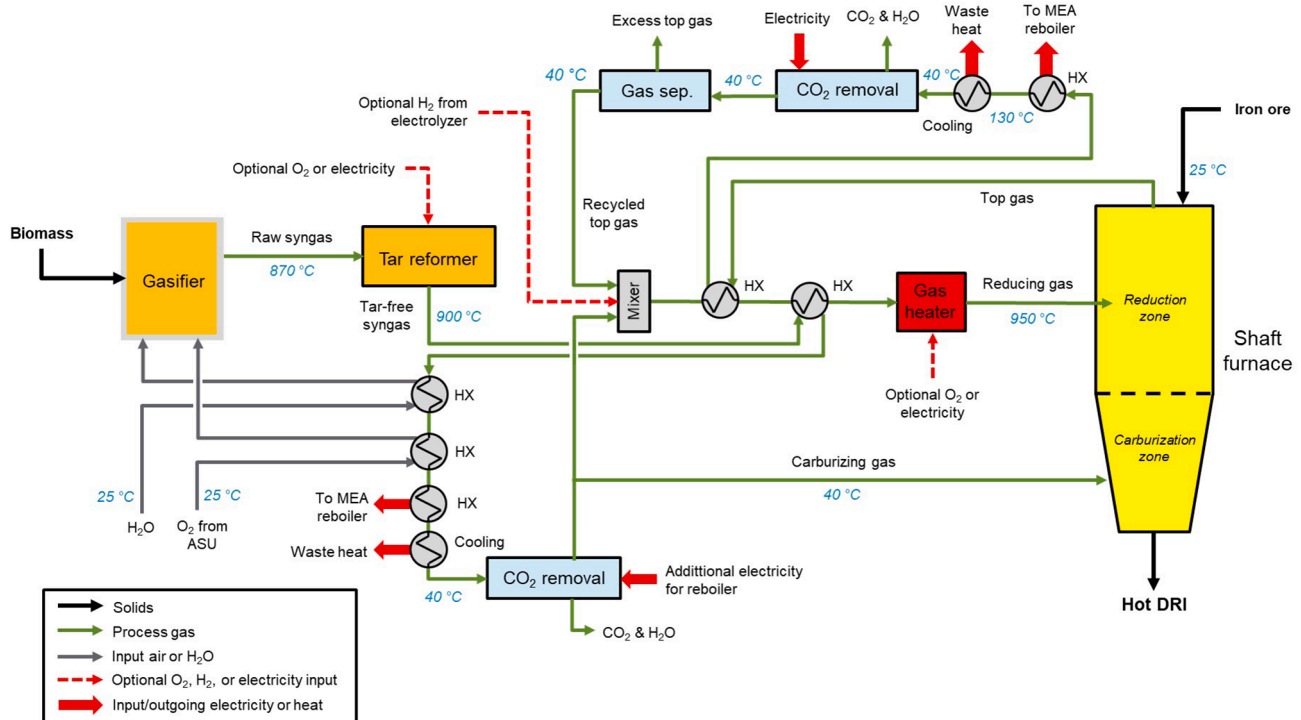
Fig. 3. Schematic diagram of the process integration based on steam/oxygen-blown CFB gasifier with a tar reformer and without biomass dryer (i.e., CFB-ASU-O$_2$, CFB-Electrolyser-O$_2$, or CFB-Electroreformer scenarios).

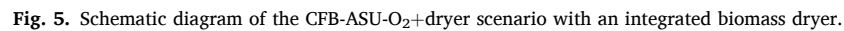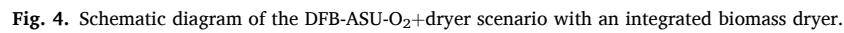converted, and the gas residence time is also limited [34]. Consequently, a thermodynamic equilibrium modelling approach tends to over-predict the yields of H$_2$ and CO and under-predict the yields of CO$_2$, light hydrocarbons, tars, and char [34]. Therefore, instead of a full equilibrium approach, a semi-empirical model is developed to simulate a steam/oxygen-blown CFB gasifier in the Aspen Plus. The model consists of RYield, RGibbs, and separator (Sep) blocks, as seen in Fig. 7.

In the model, the biomass input to the gasifier is firstly breakdown into carbon, H$_2$, O$_2$, and hydrocarbon compounds (CH$_4$, C$_2$H$_2$, C$_2$H$_4$,

C$_2$H$_6$, C$_3$H$_8$, benzene, and naphthalene), H$_2$S, and NH$_3$ by using an RYield-block. The composition of the output stream from the RYield-block is determined based on the following approach,

- the yields of hydrocarbon compounds are estimated by using empirical correlations from Hannula and Kurkela [35], which can also be seen in Table 5,

Fig. 4. Schematic diagram of the DFB-ASU-O_2+dryer scenario with an integrated biomass dryer.

Fig. 5. Schematic diagram of the CFB-ASU-O_2+dryer scenario with an integrated biomass dryer.

- the amounts of H_2S and NH_3 are determined by assuming that all fuel sulfur and nitrogen contents react to produce H_2S and NH_3, respectively [36],

- the yields of carbon, H_2 and O_2 are determined based on the elemental balance calculation,
- the composition of char is assumed to be 100 % carbon, and

Table 2

The fuel properties of biomass used for representing the wood pellets and logging residues biomass in this study [31].

Property	Value
Ultimate composition (wt%, dry basis)	
Ash	0.30
C	50.7
H	6.1
N	0.1
O	42.8
S	0.01
LHV (MJ/kg, dry-ash-free basis)	18.7

Table 3

The compositions of iron ore used in this study [32].

Materials	Value (wt.% as received)
Fe_2O_3	94.8
Fe_3O_4	1.0
Gangue (modeled as SiO_2)	2.6
Moisture content	1.6

Table 4

Description of reactor blocks used in Aspen Plus V12.

Block	Function	Examples of processes in this study
RYield	Reactor with specified yield.	Breakdown of biomass into carbon, H_2, O_2, and hydrocarbon compounds in the gasifier.
RStoic	Stoichiometric reactor with specified reactions and extent of conversion.	Combustion of fuel (excess top gas or char) in the biomass dryer and DFB's combustor.
RGibbs	Chemical and phase equilibrium by Gibbs energy minimisation.	Tar reforming in the autothermal tar reformer.
Heater	Determines thermal and phase conditions of a stream. It can be used as a heater or a cooler.	Heating of reducing gas.
HeatX	A heat exchanger between two streams.	Heat recovery between hot syngas/top gas with other cold streams.
Sep	Separate specific components from streams.	Water condenser and CO_2 removal processes.

• the amount of heat duty of the RYield-block is calculated based on the higher heating values (HHV) of the input and output streams, in which the HHV of biomass is estimated by using a correlation proposed by Channiwala and Parikh [37].

Thereafter, the output stream of the RYield-block is fed to a separator block to separate the unconverted carbon fractions, which will not be subjected to the subsequent conversion block (RGibbs-block). The amount of this unconverted carbon is calculated using the formula in Table 5. In the subsequent RGibbs-block, the remaining carbon (unreacted char), H_2, and O_2 react with the additional fluidisation steam and O_2 into syngas based on the Gibbs minimisation method. In the last step, a Sep-block is then used to separate the ash from the final syngas stream.

The developed CFB gasifier model is then validated by comparing the simulated results with the experimental data obtained from a previous study using a pressurised fluidised-bed pilot rig [35]. The validation shows that a reasonably good agreement between the experimental and simulated values by the developed model has been achieved in this study. More details and discussions on the model validation can be found in the supplementary material (section S.2).

2.3.3.2. Steam-blown DFB gasifier. The DFB gasifier is modelled by dividing the model into two sections: the combustor and the gasifier sections, as illustrated in Fig. 8. In the gasifier section, an RYield-block is used to represent the gasification process, in which the biomass is converted into non-condensable gases, tar compounds, and char. The temperature of the RYield-block is set to be the same as the temperature of biomass input. During the practical application, the circulated bed material is often oxidised in the combustor, which subsequently provides an O_2 transport into the gasifier. In the case of olivine, which is a common bed material used in the DFB, this property has been linked to its iron content that undergoes repeated oxidation–reduction cycles at a high temperature, which leads to the migration of iron to the surface and the formation of iron oxides [38]. The O_2 transport is typically undesired as it can increase the concentration of CO_2 in the syngas. The level of O_2 transport is typically in the range of 5 % of the stoichiometric demand of full combustion in the case of olivine bed material [22].

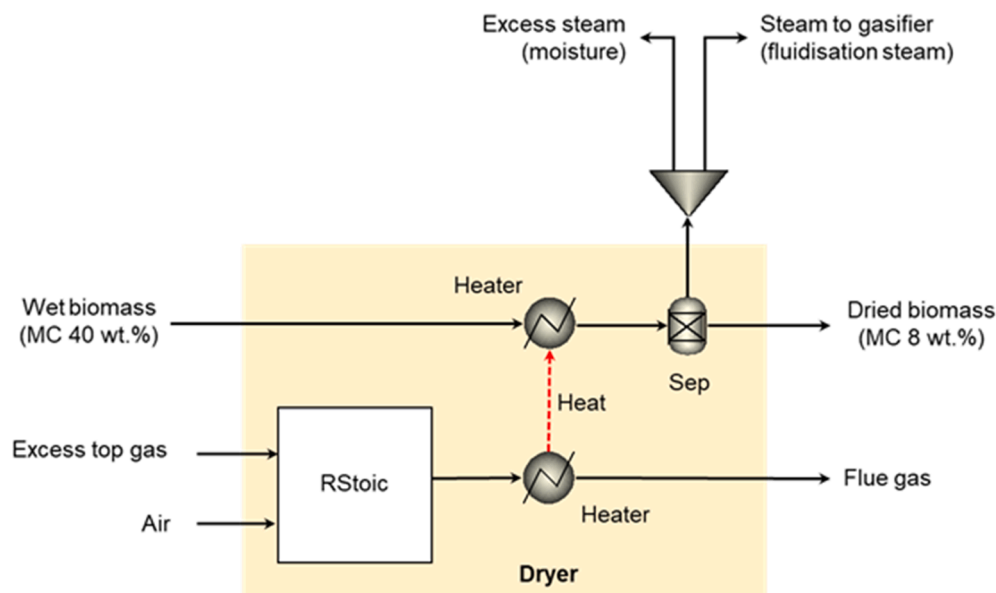The composition of the output stream from the RYield-block is determined based on the following approach,

Fig. 6. Schematic diagram of the biomass dryer model (redrawn from the actual process flowsheet used in Aspen Plus V.12).
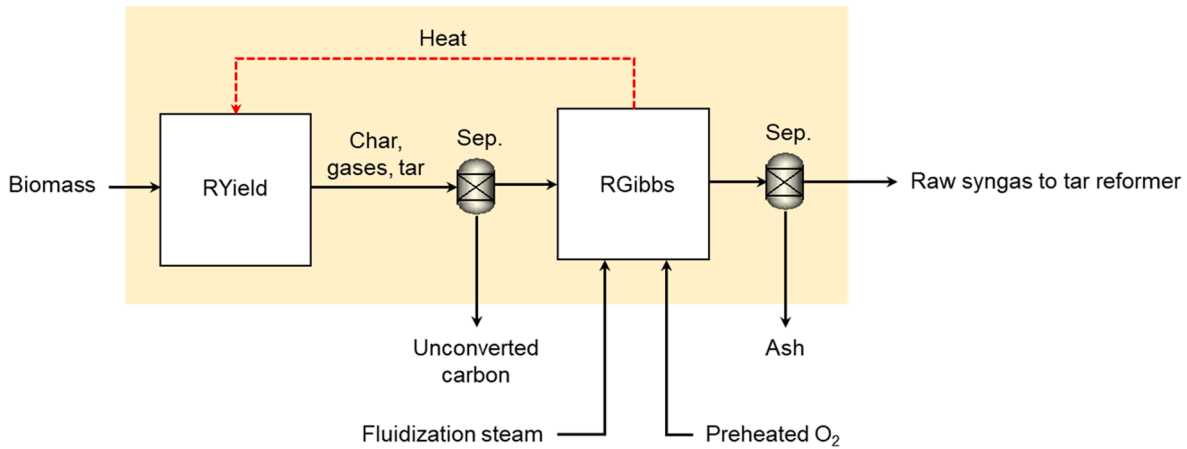
Fig. 7. Schematic diagram of the steam/oxygen-blown CFB gasifier model (redrawn from the actual process flowsheet used in Aspen Plus V.12).

Table 5
The empirical correlations for determining the yield of non-equilibrium compounds produced from the steam/oxygen-blown CFB gasifier [35].

Yields	Correlations
Carbon conversion	$0.0155 \times T + 86.068$ %
CH_4	$-0.003 \times T + 7.074$ mol kg^{-1}
C_2H_2	$-0.00004 \times T + 0.06454$ mol kg^{-1}
C_2H_4	$-0.002 \times T + 2.987$ mol kg^{-1}
C_2H_6	$-0.001 \times T + 1.196$ mol kg^{-1}
C_3H_8	$-0.000155 \times T + 0.150921$ mol kg^{-1}
C_6H_6 (benzene)	0.27 mol kg^{-1}
$C_{10}H_8$ (naphthalene)	0.3 mol kg^{-1}

T represent the gasification temperature in °C.

- the composition of char is assumed to be 100 % carbon,
- the yield of H_2, CO, CO_2, and hydrocarbon compounds are based on the results from the GoBiGas DFB plant [31], which use the same biomass feedstock as presented in Table 1, with benzene and naphthalene used to represent the BTX and heavy tar fractions, respectively,
- all fuel sulfur and nitrogen contents react to produce H_2S and NH_3, respectively [36], and
- the amount of transported O_2 to the gasifier and char yield is determined based on elemental balance calculation.

The amount of heat needed for the gasification is determined based on the HHV of the input and output streams, similar to the CFB gasifier model. After that, the output stream from RYield-block is mixed with the fluidisation steam. The temperature of this mixture steam is then

elevated by using a Heater-block to 870 °C, which is assumed to be the final temperature of the gasifier outlet. A separator (Sep-block) is then added to separate the char from the stream, which will be used for the combustor section or recovered as biochar.

In this DFB model, the required heat to maintain the gasification process at 870 °C is supplied by operating the combustor section at 920 °C. The gasification part of the existing steam DFB plants is typically operated between 800 and 870 °C [39]. In this study, the higher operating temperature of 870 °C is selected to compensate for the heat losses that are not considered, such as the heat loss due to the separation steps, filtering, etc. It should be noted that, at a commercial scale, lower gasifier temperatures are always preferred to lower the risk of technical problems such as agglomeration of bed materials, clogging due to higher release of alkali metals, etc. [39]. In the process model, the heat from the combustor is transferred to the gasifier through Heat-1 and Heat-2 streams. An RStoic-block is used to accommodate a stoichiometric combustion reaction of the input fuel. In the proposed biosyngas DRI system, the combustor can be operated using either excess top gas from DRI or char produced from the gasifier section as fuel. Maximum use of top gas is applied in the scenarios where the char will be recovered from the DFB for downstream steelmaking processes. The char from the circulating bed material can be removed using a carbon stripper [26]. In this model, the char removal is realised by using a Sep-block. Meanwhile, when char recovery is not needed, the char will be fully combusted. The total amount of required fuel for the combustor is determined to meet the energy for the gasification reactions in the RYield-block (Heat-1) and the sensible heat to reach the final syngas temperature of 870 °C (Heat-2).

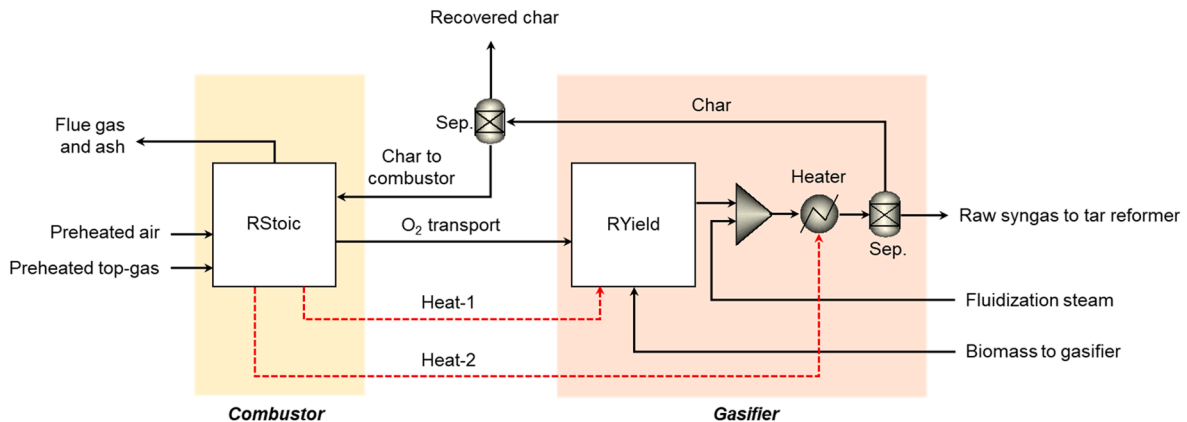The DFB model's validation is then performed using the

Fig. 8. Schematic diagram of the steam-blown DFB gasifier model (redrawn from the actual process flowsheet used in Aspen Plus V.12).

experimental data obtained from the ~ 20 MW GoBiGas demonstration plant [31]. A reasonably good agreement is found between the experimental and simulated values, as the average relative error is ~ 5 %, most likely due to the elemental balance corrections following the presence of O_2 transport and the simplified char composition of 100 % carbon. More details and discussions on the DFB model validation can also be found in the supplementary material (section S.2).

2.3.4. Tar elimination

2.3.4.1. Tar removal by a wet scrubber. As explained previously, this study considers two options for eliminating the tar content in syngas: tar reforming and the wet scrubber method. In the case of tar removal by wet scrubber, the real operating parameter data obtained from the GoBiGas demonstration plant [40] is used in the model. According to the GoBiGas plant, the wet scrubber is operated at 35 °C using rapeseed methyl esters (RME) solvent, at which the heavy tar is removed together with the condensed water. In the larger commercial-scale plant, a scrubber agent extracted from the produced tars or other less expensive solvents would be used instead of RME [41]. Subsequently, a carbon bed is added after the wet scrubber unit to remove the remaining BTX fraction. In this model, the process is simplified by using a single Sep-block to separate the BTX and heavy tar fraction from syngas. The separated heavy tar is then fed to the combustor section of the DFB gasifier to add more energy for the gasification. At the same time, the BTX fraction is recovered as a byproduct. Thereafter, the tar-free syngas is subjected to the CO_2 removal process. Fig. 9 presents the developed model of the wet tar scrubber with the subsequent CO_2 removal process. The figure shows that the hot raw syngas is first used to preheat the reducing gas through a heat exchanger before the tar removal process. After the heat exchanger, the syngas temperature is reduced to 500 – 600 °C; thus, it can be used to provide the heat needed for the MEA reboiler unit of the CO_2 removal process. In the model, the heat recovery for the MEA reboiler unit is made by a cooling step using a Heater-block.

The outgoing syngas stream from this block is assumed to be 130 °C, which is 10 °C higher than the output temperature of the MEA reboiler unit. Lastly, another cooling step further reduces the syngas temperature to the operational temperature of the wet scrubber (35 °C).

2.3.4.2. Autothermal and electrified tar reformer. The tar reformer is assumed to be either an autothermal or an electrified tar reformer. In an autothermal tar reformer, the heat needed for the endothermic reforming reactions is provided through partial oxidation of the syngas. The hot raw syngas is assumed to enter the reformer at the same temperature as the gasifier outlet (870 °C). The source of O_2 for partial oxidation is supplied by an ASU or an electrolyser. The autothermal tar reformer is modelled by using an RGibbs-block. Previous studies have demonstrated that RGibbs-block can predict the reforming products at an acceptable level [42,43]. The hydrocarbon gases, BTX, and heavy tar are assumed to be fully converted into CO, CO_2, and H_2 at an operating temperature of 900 °C. These assumptions are based on an existing autothermal tar reformer operating at the ~ 20 MW biomass CFB gasifier at Skive, Denmark [44,45]. This reformer consists of several mega-monolith metallic catalysts that allow dusty tar-rich syngas to pass through the monolithic channels [45]. The reformer can achieve nearly 100 % conversion of tar and approximately 95 % conversion of CH_4 at 850 – 920 °C [44]. The operating temperature is elevated by adding external air through three-stages combustion [44]. On the other hand, in the case of an electrified reformer, the reformer catalyst is internally heated by using electricity, instead of injecting O_2. In this reformer, the catalyst is a part of the heating element itself [16]. Despite the early-stage developments, this emerging concept has recently gained more interest due to its compact design, higher efficiency, and lower carbon footprint [16]. The electrified reforming process is achieved in the process model by setting the RGibbs-block to a fixed temperature. After the tar reforming, the tar-free syngas is fed to heat exchangers (modelled by HeatX-blocks) before being fed to the CO_2 removal process. The schematic diagram of the developed model for the tar reformer, followed
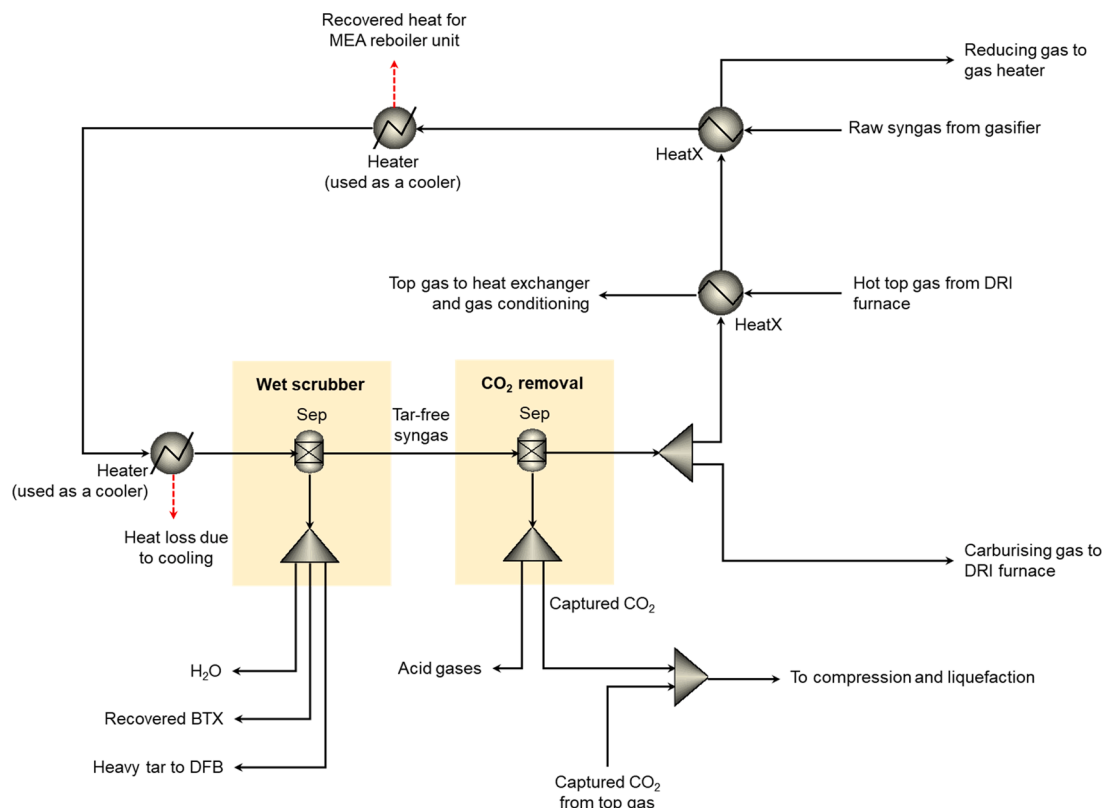
Fig. 9. Process flow diagram of the wet tar scrubber and CO_2 removal process (redrawn from the actual process flowsheet used in Aspen Plus V.12).

by a subsequent CO_2 removal process, is presented in Fig. 10.

2.3.5. CO2 removal and liquefaction

The CO_2 removal process is modelled using a Sep-block, where the CO_2 is directly separated from the syngas stream with H_2O and acid gases. A CO_2 removal rate of 95 % is assumed [40], with a CO_2 purity of 100 %. These assumptions are also applied for CO_2 removal from top gas DRI. H_2S and NH_3 are also assumed to be fully removed from the syngas. As explained previously, an MEA-based CO_2 removal is considered for this study owing to its maturity and proven commercial technology [46]; thus, reliable data on its commercial performance are readily available for this study. The total energy consumption of the CO_2 capture process can be assumed to equal the heat duty of the MEA reboiler unit, which is 3.5 MJ/kg-CO_2 [46], or equivalent to 972 kWh/t-CO_2. Part of the heat required for CO_2 removal can be supplied by using heat recovered from the system through heat integrations. In this study, the heat recovery is implemented between the reboiler unit of the MEA capture plant and the syngas or top gas streams by assuming a reboiler temperature of 120 °C [46] and a heat exchanger minimum temperature difference of 10 °C [47].

The captured CO_2 will then be liquefied at a delivery pressure of 15 bar and transported in a ship-based CCS chain. This delivery pressure is selected as it has been considered a potential candidate for a full-scale CCS chain, owing to its mature concept based on the experience of transporting CO_2 with food-grade quality [48,49]. The total CO_2 compression and cooling electricity consumption are assumed to be 105 kWh/t-CO_2 [48].

2.3.6. DRI shaft furnace

Before the DRI shaft furnace, a gas heater is required as a final heating step to elevate the temperature of the reducing gas to 950 °C, which is the typical inlet temperature of reducing gas to the natural gas MIDREX DRI furnace [50]. In the gas heater, the mixture stream of CO_2-lean syngas (i.e. syngas after CO_2 removal) and the recycled top gas is heated through partial oxidation by adding O_2 or heated by electricity. For both gas heater and DRI shaft furnace models, the recycled top gas is treated as an inert stream; thus, it does not involve any reactions throughout the process. In the case of partial oxidation, an RGibbs- and a

Heater-blocks are used to model the gas heater. The former facilitates partial oxidation reactions based on a thermodynamic equilibrium approach. In contrast, the latter is used to increase the temperature of the inert recycled top gas stream. Fig. 11 presents the process flow diagram of the gas heater (partial oxidation) and DRI shaft furnace models. Meanwhile, in the case of electric gas heater, only Heater-blocks are used to elevate the reducing gas instead of using an RGibbs-block.

In the DRI furnace, reforming reactions occur in the surrounding area of the reducing gas inlet [51]. Thus, in the developed model, the hot reducing gas is first fed to an RGibbs-block to represent this reforming step. After that, in the reduction zone, the reduction process of iron ore is modelled by using a series of RStoic-blocks, as can be seen in Fig. 11. In these blocks, the fraction of reducing gas from the newly generated biosyngas is used to reduce Fe_2O_3 and Fe_3O_4 into Fe and FeO through Eqn (1), (2), (3), (4), (5) and (6).

$$3Fe_2O_3 + H_2 = 2Fe_3O_4 + H_2O \tag{1}$$

$$Fe_3O_4 + H_2 = 3FeO + H_2O \tag{2}$$

$$FeO + H_2 = Fe + H_2O \tag{3}$$

$$3Fe_2O_3 + CO = 2Fe_3O_4 + CO_2 \tag{4}$$

$$Fe_3O_4 + CO = 3FeO + CO_2 \tag{5}$$

$$FeO + CO = Fe + CO_2 \tag{6}$$

$$\frac{H_2O}{H_2 + H_2O} = 0.31 \tag{7}$$

$$\frac{CO_2}{CO + CO_2} = 0.42 \tag{8}$$

In the reduction zone, the Fe_2O_3/Fe_3O_4 is firstly reduced to Fe assuming that the reactions reach their equilibrium state. Therefore, the gas products from the reactions should meet the equilibrium constants that can be defined by Eq. (7) and Eq. (8). These values correspond to the equilibrium gas concentrations at ~ 670 °C [52], which is selected based on a preliminary simulation work to estimate the gas temperature after
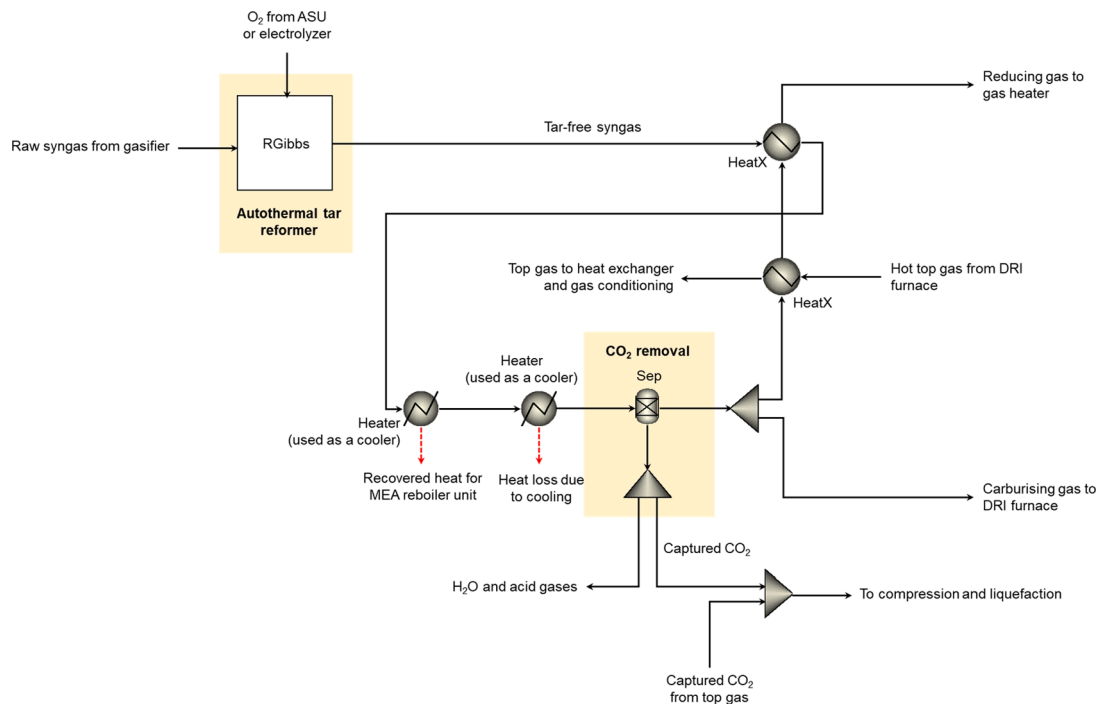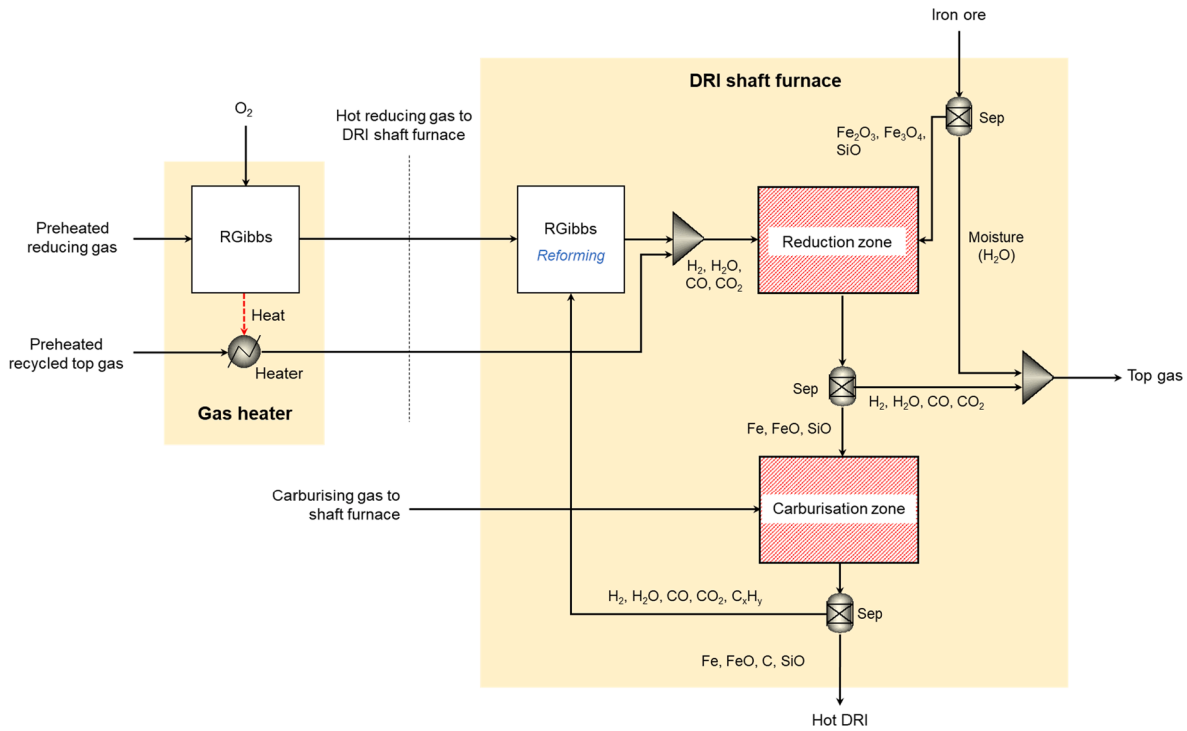
Fig. 10. Process flow diagram of the autothermal tar reformer and CO_2 removal process (redrawn from the actual process flowsheet used in Aspen Plus V.12).

Fig. 11. Process flow diagram of the gas heater (partial oxidation) and DRI shaft furnace models (redrawn from the actual process flowsheet used in Aspen Plus V.12).

full reductions of iron ore. In this model, those equilibrium constants in the process are achieved by adjusting the amount of the recycled top gas and the amount of iron ore input to the DRI furnace. Thereafter, a reverse reaction of Fe to FeO is used to set the mass fraction of FeO at the outlet of reduction zone equal to 0.08 to meet the targeted metallisation percentage of 92%.

$$2CO = C + CO_2 \tag{9}$$

$$CO + H_2 = C + H_2O \tag{10}$$

$$CH_4 = C + 2H_2 \tag{11}$$

The output stream of the reduction section is then fed to a Sep-block to separate the solid and the gas fractions. The gas fraction is discharged from the DRI furnace as a top gas. Meanwhile, the solid fraction (Fe, FeO, and inerts) is subjected to the carburisation zone (modelled by an RStoic-block), representing the carburisation zone at the lower part of the shaft furnace. The carburising gas is assumed to enter the carburisation zone at the same discharge temperature of the MEA CO_2 removal unit (40 °C). A carbon content of 2 % in the DRI product is aimed at after the carburisation, which is achieved by adjusting the ratio of the biosyngas that go as a carburising gas. The assumed reactions for the carburisation process are presented in Eq. (9) – (11) [53]. Thereafter, the excess gas after the carburisation flows upward to the reduction zone, as can be seen in see Fig. 11, whereas the final DRI product is discharged from the furnace. In most cases in this study, CO is the main component of the carburising gas; thus, a hot DRI is produced as the CO-based carburisation reactions are exothermic. Based on the simulation results, the temperature of the hot DRI ranges between 760 and 790 °C, which is similar to the case of coal gasification DRI furnaces [54]. The summary of the operating parameters of the biosyngas DRI production system is listed in Table 6.

2.3.7. Evaluation of the system performance

In this study, different integration scenarios of biosyngas DRI route are proposed. The performance of those integration scenarios is evalu-

ated based on both total gross ($E_{DRI-gross}$) and net energy demand ($E_{DRI-net}$), which are presented in kWh/t-DRI and can be defined by the following equations,

$$E_{DRI-gross} = E_{biomass} + E_{electric} \tag{12}$$

$$E_{DRI-net} = E_{biomass} + E_{electric} - E_{top-gas} - E_{waste-heat} - E_{Fe} - E_{char} - E_{BTX} \tag{13}$$

where $E_{biomass}$ is the chemical energy of biomass on an LHV basis; $E_{electric}$ is the total electricity consumption of the ASU, electrolyser, tar reformer, gas heater, MEA reboiler of the CO_2 removal unit, and CO_2 liquefaction unit; $E_{top-gas}$ is the chemical energy of excess top gas in LHV basis; $E_{waste-heat}$ is the unrecovered waste heat from low-temperature streams (i.e., cooled syngas, top gas, and flue gas after heat exchanger); E_{Fe} is the sensible heat of hot DRI; E_{char} is the chemical energy of recovered char in LHV basis; and E_{BTX} is the chemical energy of recovered BTX fraction in LHV basis (represented by the LHV of benzene).

The thermal efficiency of DRI production (η_{DRI}) is also introduced to evaluate the proposed biosyngas DRI system, which is defined as follows,

$$\eta_{DRI} = \frac{E_{Fe}}{E_{DRI-gross}} \tag{14}$$

where E_{Fe} represents the chemical energy stored in the reduced ore. This energy is determined as the heat of oxidation of FeO_X in the hot DRI into Fe_2O_3, which is assumed to be 1912 kWh/t-FeO_X at a metallisation degree of 92 % [22].

3. Results and discussion

3.1. Quality of the reducing gas

The DFB and CFB gasifiers differ mainly in the supply of the required heat to meet the demand of the endothermic gasification reactions. In DFB gasifiers, the heat is supplied by externally combusting parts of the produced char or syngas in the combustor section. As the major part of

Table 6

Summary of the operating parameters and assumptions for each different process module.

Process	Operating parameters	Ref.
Drying		
Biomass feed temperature	25 °C	
Discharge temperature of biomass and steam	130 °C	
Final moisture content	8 wt%	
Steam DFB gasification		
Gasifier	870 °C; atmospheric pressure	[31]
Combustor	920 °C; atmospheric pressure	[31]
Fluidisation steam for gasifier	0.5 kg/kg$_{dry\text{-}ash\text{-}free\ biomass}$	[40]
Air-to-fuel ratio for combustor	1.2	
Heat loss	2.5 % of fuel LHV (0.625 % for the gasifier; 1.875 % for the combustor)	[3140]
Oxy-fuel CFB gasification		
Gasifier	870 °C; atmospheric pressure	
Heat loss	2.5 % of fuel LHV	[40]
Tar wet scrubber		
Temperature	35 °C	[40]
Tar reformer		
Temperature	900 °C	[44]
Tar conversion rate	100 %	[44]
Heat loss	2.5 % of fuel LHV	
MEA CO_2 removal unit		
Absorber column temperature	40 °C	[46]
Reboiler temperature	120 °C	[46]
Removal rate	95 %	[40]
CO_2 stream purity	100 %	
Energy demand (equal to reboiler duty)	972 kWh/t-CO_2	[46]
CO_2 liquefaction		
Delivery pressure	15 bar	[48,49]
Electricity demand	105 kWh/t-CO_2	[48]
Gas heater		
Outlet temperature	950 °C	[51]
Heat loss	1 % of fuel HHV	[55]
DRI shaft furnace		
Degree of metallisation	92 %	
Carbon content of hot DRI	2 %	
Heat loss	2.5 % of Fe/FeO energy content	[22]
Heat exchangers		
Minimum temperature difference	10 °C	[47]
Air separation unit (ASU)		
Electricity demand	250 kWh/t-O_2	[56]
Electrolyser		
Power-to-H$_{2\text{-}LHV}$ efficiency	63 %	[57]

Table 7

The composition of raw syngas and tar-free syngas obtained from the process simulation of different scenarios.

	Composition of syngas (mol%)			
	DFB-ASU-O_2	DFB-ASU-O_2 + dryer	CFB-ASU-O_2	CFB-ASU-O_2 + dryer
Raw syngas from the gasifier				
H_2	27.5	27.5	20.7	22.5
H_2O	34.4	34.4	36.3	34.5
CO	16.5	16.5	13.9	15.0
CO_2	13.7	13.7	21.1	20.0
CH_4	5.9	5.9	5.3	5.3
C_2H_2	0.08	0.08	0.04	0.04
C_2H_4	1.37	1.37	1.52	1.52
C_2H_6	0.13	0.13	0.41	0.41
Benzene	0.27	0.27	0.32	0.32
Naphthalene	0.10	0.10	0.35	0.35
Tar-free syngas after tar reformer				
H_2	38.1	38.1	31.7	33.1
H_2O	26.9	26.9	28.2	26.8
CO	22.4	22.4	23.5	24.4
CO_2	12.6	12.6	16.6	15.7

the combustion reaction occurs outside the gasifier chamber, the generated syngas has a higher quality than CFB gasifiers in terms of the higher concentration of H_2 and CO, and lower concentration of CO_2. Table 7 presents the composition of raw syngas and tar-free syngas obtained from the DFB-ASU-O_2, DFB-ASU-O_2+dryer, CFB-ASU-O_2, and CFB-ASU-O_2+dryer scenarios. The table shows that the H_2 and CO concentration in the raw syngas from DFB-based scenarios are 27.5 and 16.5 mol%, respectively, which are higher than that of CFB-based scenarios ($H_2 \leq 22.5$ mol%, CO ≤ 15.0 mol%). In the case of CFB gasifier, the heat demand is met by partial oxidation inside the gasifier chamber; thus, syngas produced from the CFB gasifier has a higher CO_2 concentration between 20 and 21 mol%.

In the process simulation, the tar reformer is assumed to be in thermodynamical equilibrium with a tar conversion rate of 100 %, nearly the same as the conversion rate value obtained from the current large-scale tar steam reformer [44]. Thus, the hydrocarbon gases and the tar compounds (represented by benzene and naphthalene) are fully converted into H_2, H_2O, CO, and CO_2. The composition of the tar-free syngas after the tar reformer obtained from the process simulation is presented in Table 7. Like raw syngas, the tar-free syngas of the DFB-

based scenarios generally has a higher H_2 and a lower concentration of CO_2.

RP (defined as the molar ratio of (H_2 + CO)/(H_2O + CO_2)) is the main key parameter to evaluate the quality of the reducing gas derived from the biosyngas. Specifically, the value of the RP should not be lower than that of existing gas-based DRI processes. The reducing gas used in the existing natural gas-based MIDREX process is known to have RP values higher than 9 [27]. As seen in Table 8, the RP value of the syngas after the tar removal/reforming process is very low (<3.2). After the CO_2 removal process, the value can be significantly increased to 64.3–147.5 following the CO_2 and H_2O separation from the syngas. Finally, the RP value of the hot-reducing gas entering the shaft furnace is at least higher than 12.6. This value is higher than the normal value in the existing natural gas-based DRI process. In addition, using an electrified tar reformer and gas heater can significantly optimise the RP value of the reducing gas, as demonstrated by the results of the DFB-Electroreformer (RP = 111.8) and CFB-Electroreformer (RP = 89.3) scenarios. This is due to the absence of partial oxidation reactions in both electrified reactors; thus, the formation of CO_2 and H_2O can be suppressed, leading to a higher RP value.

The H_2/CO ratio is another key parameter to assess the reducing gas quality. The reducing gas used in the DRI shaft furnaces can have a wide range of H_2/CO ratio values. Natural gas MIDREX DRI furnaces typically use a reducing gas with an H_2/CO value of around 1.6. Meanwhile, DRI processes that use reducing gas from coal gasification often have lower values of H_2/CO ratio below 0.2 [54]. As seen in Table 8, the simulation results show that the H_2/CO ratio of the hot-reducing gas entering the DRI shaft furnace ranges between 1.31 and 2.67, depending on the different integration scenarios. These values are comparable with the typical values found in the natural gas MIDREX DRI process and significantly higher than the coal gasification MIDREX process. The highest value of H_2/CO is obtained in the case where an electrolyser is used in the system, which can reach 2.61 for DFB-Electrolyser-O_2 and 2.67 for CFB-Electrolyser-O_2.

According to the results above, it has been demonstrated that the proposed biomass gasification, with the subsequent syngas conditioning system, can produce a reducing gas with a sufficient quality to be used in a typical gas-based DRI furnace.

3.2. Captured CO_2

The energy demand and the amount of captured CO_2 for different biosyngas DRI integration scenarios are presented in Table 9. In general,

Table 8

The reduction potential (RP) and H_2/CO ratios of gases obtained from the process simulation.

Scenarios	Syngas after tar removal/reforming		Syngas after CO_2 removal		Hot reducing gas to shaft furnace[a]		Top gas	
	RP[b]	H_2/CO	RP[b]	H_2/CO	RP[b]	H_2/CO	RP[b]	H_2/CO
DFB-Scrubber	3.2	1.67	64.3	1.67	16.8	1.62	1.8	2.04
DFB-ASU-O_2	1.5	1.70	96.3	1.70	13.9	1.66	1.9	1.98
DFB-Electrolyser-O_2	1.5	1.70	96.3	1.70	12.6	2.61	2.0	3.02
DFB-Electroreformer	2.3	1.74	147.5	1.74	111.8	1.74	1.9	2.03
DFB-ASU-O_2+dryer	1.5	1.70	96.3	1.70	13.8	1.66	1.9	1.96
CFB-ASU-O_2	1.2	1.35	66.6	1.35	13.6	1.31	1.8	1.55
CFB-Electrolyser-O_2	1.2	1.35	66.3	1.35	13.3	2.67	1.9	3.07
CFB-Electroreformer	1.9	1.38	103.6	1.38	89.3	1.38	1.8	1.60
CFB-ASU-O_2+dryer	1.4	1.36	73.5	1.36	13.5	1.66	1.8	1.58

[a] After mixing with recycled top-gas and H_2 from electrolysis, and a temperature rise to 950 °C.

[b] defined as a molar ratio of $(H_2 + CO)/(H_2O + CO_2)$.

the amount of captured CO_2 linearly correlates with biomass consumption. Using higher electricity consumption for producing reducing gas would decrease biomass consumption, leading to a lower specific amount of CO_2 generation and capture. For instance, the electrolyser addition, as proposed in DFB-Electrolyser-O_2 and CFB-Electrolyser-O_2 scenarios, reduces the amount of the captured CO_2 by 22 and 32 % compared to DFB-ASU-O_2 and CFB-ASU-O_2, respectively. These values correspond to the reduction in the specific biomass consumption by 19–28 % when an electrolyser is added to the system. In these cases, adding H_2 from the electrolyser leads to a lower concentration of CO_2 in the top gas before the capture process owing to the lower CO content in the reducing gas. Meanwhile, electrification of the tar reformer and gas heater prevents the combustion of CO in the syngas; hence, it can further reduce the amount of generated and captured CO_2 to a similar level as the electrolyser scenarios. A slightly lower amount of captured CO_2 is found in the DFB-scrubber scenario than DFB-ASU-O_2 despite the slightly higher biomass consumption as some parts of carbon are extracted from the system as chemical byproducts (i.e., BTX fraction of raw syngas).

The steam/oxygen-blown CFB scenarios (0.79–1.13 t-CO_2/t-DRI) generally have higher amounts of captured CO_2 than the steam-blown DFB scenarios (0.65–0.91 t-CO_2/t-DRI). This is because, in this study, the capture of CO_2 in the flue gas stream from the DFB's combustor is not considered as it complicates the process. Examples of the mass balance diagrams of the production systems are depicted in Fig. 12(a) and Fig. 13 (a), representing the simulation results of DFB-ASU-O_2+dryer and CFB-ASU-O_2+dryer scenarios, respectively. As seen in Fig. 12(a), the combustion part of the DFB gasifier releases a 1.260 t/t-DRI of flue gas which contains 0.260 t/t-DRI of CO_2 being released into the air. This value corresponds to 25 % of the total amount of generated CO_2 from the process. In contrast, as seen in Fig. 13(a), the DRI production using a CFB gasifier only releases<3 % of the generated CO_2 to the air, which comes from the combustion in the drying process, whereas the rest of the CO_2 (>97 %) is captured from the syngas and recycled top gas. To summarise, CFB gasifiers tend to provide higher CO_2 separation in the DRI production system; however, it is likely followed by the increase in the energy demand of the ASU and CO_2 capture unit, as described further in the discussion below.

3.3. Energy demand and efficiency

Within the CFB-based production systems, the higher amount of CO_2 that needs to be separated from syngas and top gas streams causes a higher overall energy demand than in the DFB-based scenarios. From Table 9, it can be seen that the gross energy demand ($E_{DRI-gross}$) needed for CFB scenarios are generally 7–11 % higher than the steam DFB scenarios. Specifically, more electricity consumption is required owing to the higher energy duty of the MEA reboiler unit and CO_2 liquefaction. For instance, CFB-ASU-O_2 requires 960 kWh/t-DRI for its MEA reboiler and CO_2 liquefaction unit, which is doubled that of DFB-ASU-O_2, despite

the only 24 % increase in the amount of captured CO_2. In addition, a relatively smaller rise in ASU electricity demand is observed in the case of CFB-based systems due to the higher O_2 consumption. In terms of thermal efficiency (η_{DRI}), CFB-based systems consequently have slightly lower values than DFB-based systems, as they are between 38.5 and 43.1 %, while the η_{DRI} values of DFB-based scenarios are between 41.2 and 49.6 %.

Electrified technologies can either lower or increase the overall energy demand, which largely depends on their efficiency. In this study, the results of the process simulation show that the cold gas efficiency of the gasifiers (i.e., the ratio of the LHV of raw syngas to the LHV of dry biomass input) ranges between 84 and 88 %. These values are notably higher than the electrolyser's efficiency value assumed in this study (63 %). Consequently, adding an electrolyser to the DRI production system increases the overall energy demand of the system. For instance, as demonstrated by DFB-Electrolyser-O_2, adding more H_2 produced from an electrolyser to the reducing gas can decrease the $E_{biomass}$ value by 20 % (or 719 kWh/t-DRI lower) than that of DFB-ASU-O_2. This reduction is then followed by a significant increase in electricity consumption of 1001 kWh/t-DRI, which lead to a 7 % in the value of $E_{DRI-gross}$. Overall, the electrolyser scenarios consume the highest amount of electricity compared to other scenarios, as the $E_{electric}$ value ranges between 1501 and 2213 kWh/t-DRI. On the other hand, the electrification of the tar reformer and gas heater results in a further reduction of biomass consumption with a relatively lower electricity consumption than that of electrolyser scenarios. For instance, the $E_{biomass}$ value of DFB-Electroreformer is 26 % lower (931 kWh/t-DRI lower) than that of DFB-ASU-O_2, followed by only a 472 kWh/t-DRI increase in electricity demand, which leads to the lowest $E_{DRI-gross}$ value. This low level of energy demand is possible as the efficiency of the electrified reformer considered in the process simulation is > 93 %. Correspondingly, electrification of the reformer exhibits the highest overall system efficiency as the value of η_{DRI} can reach 49.6 and 45.7 for DFB-Electroreformer and CFB-Electroreformer, respectively. However, it should be noted that in this study, no further optimisation is carried out for each scenario, which may result in different energy demand values and overall efficiency of the systems. The ratio of the electricity-to-biomass energy is also an interesting aspect to evaluate, as the two energy carriers have different exergy content. In the electrolyser-based system, the electricity-to-biomass is 0.52–0.89, which is higher than that of electrified reformer cases (0.36–0.55).

Table 9 also presents the energy demand of the DRI production system with an integrated biomass dryer. In general, there is enough excess top gas to provide heat for the biomass dryer with a biomass moisture content of 40 %. The dryer requires approximately 330–390 kWh/t-DRI to evaporate the moisture content of biomass, which can be supplied by 64–69 % of the available excess top gas. The value of $E_{DRI-gross}$ does not notably change compared to the scenarios without biomass dryer, despite the new energy demand to evaporate the biomass moisture content. In the case of DFB-ASU-O_2+dryer, the $E_{DRI-gross}$ value

Table 9

The energy demand and amount of captured CO_2 for different integration scenarios. The biomass energy demand ($E_{biomass}$) is calculated based on the LHV of biomass on a dry basis.

Scenarios	Biomass demand (t/t-DRI)[a]	$E_{biomass}$ (kWh/t-DRI)	$E_{electric}$ (kWh/t-DRI)							$E_{DRI-gross}$ (kWh/t-DRI)	$E_{DRI-net}$ (kWh/t-DRI)	η_{DRI}	Captured CO_2 (t/t-DRI)
			ASU	Electrolyser	Tar reformer	Gas heater	MEA reboiler[b]	CO_2 liquefaction	Total				
DFB-Scrubber	0.72	3722	33				382	92	507	4229	3021	42.8	0.88
DFB-ASU-O$_2$	0.69	3604	45				359	96	500	4105	3152	44.1	0.91
DFB-Electrolyser-O$_2$	0.56	2885		1203			224	74	1501	4386	3252	41.2	0.71
DFB-Electroreformer	0.52	2673			317	310	278	68	972	3645	2835	49.6	0.65
DFB-ASU-O$_2$+dryer	0.69	3565	45				271	95	411	3976	3102	45.5	0.90
CFB-ASU-O$_2$	0.67	3492	99				841	119	1059	4551	3472	39.7	1.13
CFB-Electrolyser-O$_2$	0.48	2481		1621			511	81	2213	4695	3422	38.5	0.77
CFB-Electroreformer	0.49	2555	38		370	297	612	83	1400	3955	3046	45.7	0.79
CFB-ASU-O$_2$+dryer	0.65	3388	91				607	114	812	4200	3345	43.1	1.09

[a] On dry basis.
[b] Additional electricity consumption needed for the MEA reboiler unit for CO_2 removal.

slightly decrease by 3 % compared to that of DFB-ASU-O$_2$ scenario, while CFB-ASU-O$_2$+dryer exhibits an 8 % lower value of $E_{DRI-gross}$ than that of CFB-ASU-O$_2$ scenario. Additionally, around 18–23 % reduction in the electricity demand is observed compared to the scenario without biomass dryer. The reason for this reduction is that in the scenarios with biomass dryer, more available heat can be recovered for heating the MEA reboiler unit. Thus, the additional electricity input needed for the reboiler unit can be reduced. With this reduction in the energy demand, the η_{DRI} value of CFB-ASU-O$_2$+dryer is notably higher (43.1 %) than CFB-ASU-O$_2$ (39.7 %).

A sensitivity analysis is performed to investigate the effect of lowering the reforming temperature (from its original temperature of 900 °C) on the overall energy demand for producing DRI using the proposed biosyngas system. The sensitivity analysis is carried out at reforming temperatures of 800, 850, and 900 °C for the CFB-ASU-O$_2$+dryer case and assumes that the conversion rate of tar achieves 100 % at this temperature range. The results show that lowering the reforming temperature can reduce the O$_2$ demand of the reformer following the lower heat duty of the reformer. Nevertheless, this reduction is also followed by increased heat and O$_2$ demands for the reducing gas heater due to the lower amount of recovered heat. As a result, the ASU electricity consumption remains similar, and no notable effects on the overall energy demand of DRI production are observed. More details on the sensitivity analysis are provided in the Supplementary Material.

It can also be seen from Table 9 that the value of $E_{DRI-net}$ is notably lower than $E_{DRI-gross}$ (by ~ 22 %), which indicates a possible further optimisation of the integration system to reduce the energy demand. As illustrated by the energy balance diagrams in Fig. 12(b) and Fig. 13(b), the syngas and top gas streams entering the cooling process at 130 °C contain a notable amount of sensible heat equal to about 210–240 kWh/t-DRI. Instead of just discharging the heat through a conventional cooler, heat pump applications can be an option to recover this low-temperature heat. As proposed by a previous study [58], the heat pumps can be used to recover the low-quality heat for heating an MEA reboiler used in the CO_2 removal process. Alternatively, these streams can also be used to supply the heat needed by the biomass dryer through further integration by heat exchangers [33]. Another potential heat recovery is the sensible heat of the hot DRI (~180 kWh/t-DRI), which can heat the biomass dryer, MEA reboiler unit, or preheat the iron ore pellets. The remaining cooling of process gas streams at above 60 °C can also be done for additional revenue through district heat production [59]. A further assessment is required to carefully consider those potential options based on the economic feasibility of the resulting process.

A benefit of the DFB gasifier is the possibility of recovering biochar from the gasifier by using a carbon stripper [26]. The recovered biochar can be used for the subsequent steelmaking processes; thus, it can also potentially decarbonise the downstream steelmaking processes by replacing the conventional fossil-based coke. To assess the possibility of this biochar recovery, a further simulation based on DFB-ASU-O$_2$+dryer scenario is carried out, in which the excess top gas is fully combusted to provide the required heat for the DFB gasifier. As a result, a part of the char produced from the gasifier section of DFB can then be recovered instead of being fully combusted in the combustor section. The simulation results show that the remaining amount of top gas (i.e., after being used for heating the biomass dryer) is not sufficient to heat the DFB gasifier fully. Thus, a significant portion of char is still required for the DFB's combustor section. It is found that 0.017 t/t-DRI of char can be recovered, while 0.056 t/t-DRI char is needed for the combustor.

3.4. Comparison with other iron production routes

From the results of this study, it can be seen that the proposed biosyngas DRI route demonstrates a competitive energy demand. Table 10 compares typical ironmaking routes, including several emerging low-

(a) Mass balance
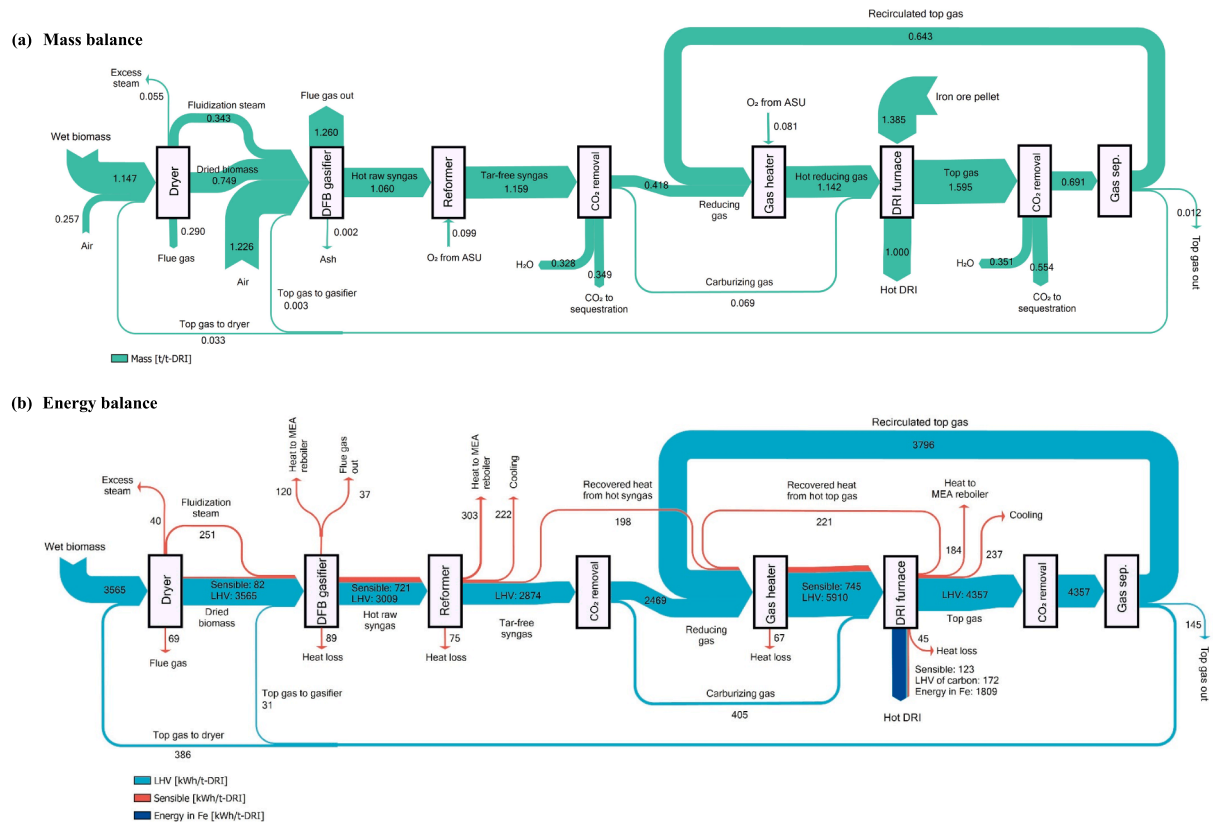
(b) Energy balance

Fig. 12. (a) Mass and (b) energy balance diagram of the DRI production system using a steam-blown Dual Fluidised Bed gasifier and an integrated biomass dryer (i. e., DFB-ASU-O_2+dryer scenario). The ASU and MEA reboiler units are not included in the diagram.

(a) Mass balance
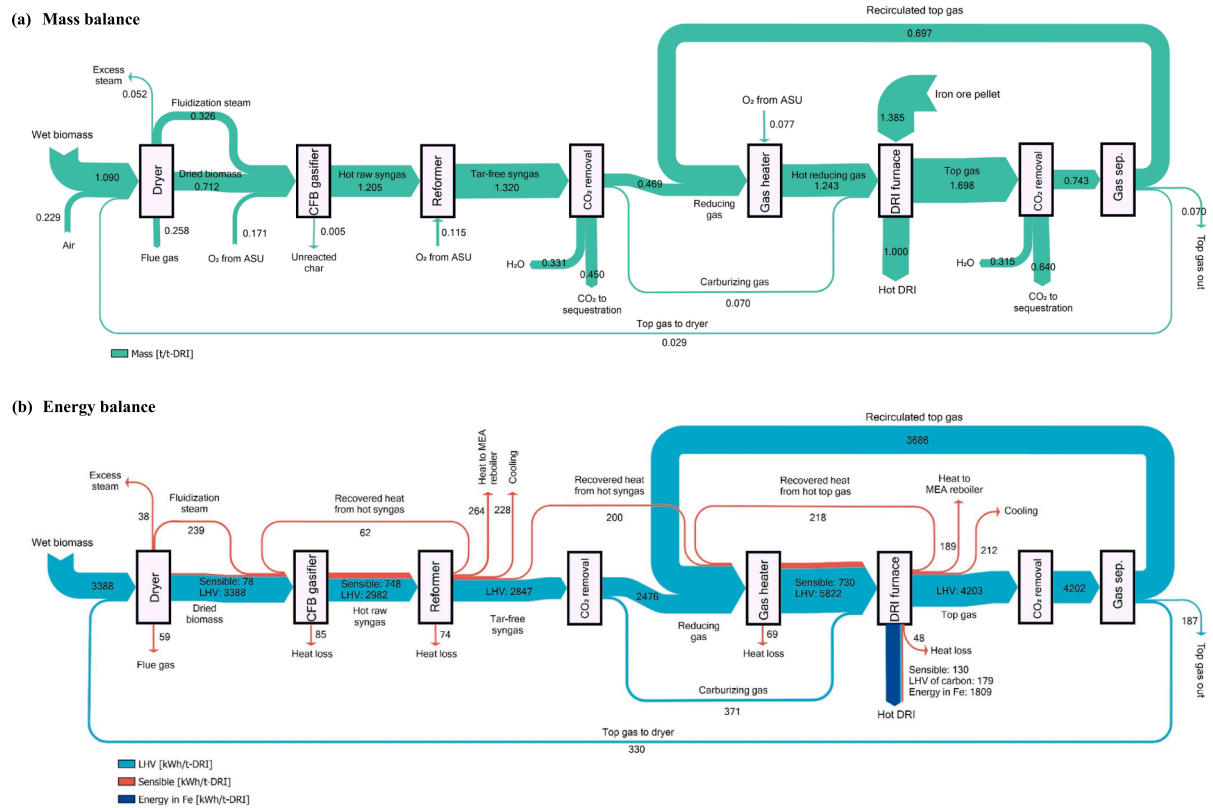
(b) Energy balance

Fig. 13. (a) Mass and (b) energy balance diagram of the DRI production system using an oxygen/steam-blown Circulating Fluidised Bed gasifier and an integrated biomass dryer (i.e., CFB-ASU-O_2+dryer scenario). The ASU and MEA reboiler units are not included in the diagram.

carbon production routes, in terms of energy demand and CO_2 generation. As seen in the table, the gross fuel energy demand of the biosyngas DRI route ranges between 3400 and 3600 kWh/*t*-DRI, according to the scenarios with lower electricity consumption and an integrated biomass drying (i.e., DFB-ASU-O_2+dryer and CFB-ASU-O_2+dryer scenarios). This fuel demand is comparable with that of existing MIDREX plants, which typically consume 3250 kWh/*t*-DRI of natural gas as reducing gas and heating fuel [60], and obviously lower than the typical fuel demand of blast furnaces (5916 kWh/*t*-hot metal) [4,61]. Comparable fuel demand is also shown in the coal-based MIDREX (MXCOL) plant, which uses ~ 3300 kWh/*t*-DRI of high-ash coal as the main fuel for reducing gas generation through a Lurgi gasifier [54]. The comparison to the MXCOL plant is interesting, especially due to the similar concept of using two CO_2 removal processes for upgrading the upstream syngas from the gasifier and the recycled top gas. Nevertheless, these comparisons should be considered carefully as the data of the fossil-based DRI above are taken from real commercial plants (see Table 10) rather than process simulation studies.

The proposed biosyngas route can be a promising alternative to the other fossil-free ironmaking routes regarding energy demand. For example, as seen in Table 10, the biosyngas route consumes a significantly lower biomass feedstock than the biochar-based DRI production route using a rotary hearth furnace, which needs a ~ 6850 kWh/*t*-DRI or 0.80 t/*t*-DRI of biochar [13,62]. This means that such a biochar DRI route would require approximately 3.20 t/*t*-DRI of biomass (on a dry basis) or 5 times larger than that of the proposed biosyngas route, considering that typically 24 % of biomass weight can be converted into biochar through a pyrolysis process [5]. Other studies have also reported the potentially higher biomass consumption in the biochar-based blast furnace process that would need up to 0.45 t/*t*-DRI of biochar to partly replace fossil fuel coke [10]. Furthermore, the total energy demand of the biosyngas route is also competitive with the currently emerging H_2 DRI production route that is predicted to consume 3600 kWh/*t*-DRI of electricity power [57]. The reported value corresponds to the gross energy demand of a H_2 DRI production system with a typical electrolyser efficiency of 63 % (LHV basis). It is also worth noting the benefit of

obtaining carbon in the DRI when biosyngas is used as a reductant agent when it comes to further processing in electric arc furnaces (EAF), in contrast to using H_2 reducing agent, which produces DRI with 0 % carbon. Carbon source is crucial in EAF and typically added in the form of in-situ carbon from DRI or scrap (c-DRI) and charge carbon (e.g., coal and coke) [63]. It provides additional energy in EAF and acts as a slag-foaming agent. Compared to the charge carbon, c-DRI has more benefits in terms of higher combustion efficiency and the absence of ash, sulfur, and volatiles, which are normally detrimental to the melting process and steel quality [64]. Thus, by using low- or high-carbon DRI from the biosyngas production route, EAF would need less charge carbon and less energy demand compared to using 0 % carbon DRI [64]. At the same time, there is no requirement for reconfiguring the operating procedures and parameters of EAF [64].

The proposed biosyngas route's energy demand can be reduced further considering the notable amount of energy in the unrecovered heat/fuel streams (e.g., the excess top gas, steam, etc.). There are approximately 850 kWh/*t*-DRI of unrecovered energy in both biosyngas scenarios (see energy balance diagram in Fig. 12 and Fig. 13). Hypothetically speaking, if this available energy can be fully used to reduce the biomass fuel consumption, this will result in a minimum fuel demand of 2500–2700 kWh/*t*-DRI, which would make the biosyngas DRI route an attractive solution for producing fossil-free DRI. This number is close to the hypothetical net energy demand of such H_2 DRI production route, which reportedly can reach 2300–2500 kWh/*t*-DRI when waste heat can be fully recovered [57]. In addition, with that same level of energy demand, ones should also consider the benefit of the proposed biosyngas system in providing carbon-negative emission when the captured CO_2 is stored, which can notably contribute to the economic and environmental aspects of the system.

Further optimisation should also be focused on reducing the energy demand for the CO_2 capture unit to make the proposed biosyngas DRI route more competitive. As shown by Table 10, the biosyngas system demand 400–800 kWh/*t*-DRI of electricity, which is significantly higher than other iron production routes as they typically only consume < 200 kWh of electricity per t iron. The major part of the electricity

Table 10

Comparison of the proposed biosyngas DRI route with other iron production routes.

Iron production route	Ref.	Type of study	Energy demand for iron production (kWh per t iron)			CO_2 generation (t CO_2 per t iron)		Notes
			Fuel	Electricity	Total	Released	Captured	
Biosyngas DRI with DFB gasifier	This work	Process simulation	3565	411	3976	0.30	0.90[a]	• Gross energy demand of DFB-ASU-O_2+dryer scenario
Biosyngas DRI with CFB gasifier	This work	Process simulation	3388	812	4200	0.03	1.09[a]	• Gross energy demand of CFB-ASU-O_2+dryer scenario
Blast furnace	[4,61]	Real plant data	5916		5916	1.37		• The total energy demand and CO_2 emission are obtained from the coke plant, sinter plant, pellet plant, and blast furnace.
MIDREX natural gas DRI	[60]	Real plant data	3250	130	3380	0.62		• A DRI production in a shaft furnace using syngas produced from a steam reformer of natural gas.
MIDREX coal-gasification DRI (MXCOL)	[54]	Real plant data	3334	175	3509			• A DRI production in a shaft furnace using syngas produced from a Lurgi gasifier. • The fuel energy demand is estimated based on the coal consumption of 0.75 t/*t*-DRI [54] and LHV coal of 16 MJ/kg.
Circofer coal-gasification DRI	[60]	Process simulation	6728	112		0.71	0.83[b]	• DRI production using a fluidised bed furnace. • A CO_2 removal unit is used to upgrade the recycled top gas. • The fuel energy demand is estimated based on the consumption of coal (0.27 t/*t*-DRI) and natural gas (0.32 t/*t*-DRI) [60].
Green H_2 DRI	[57]	Process simulation		3600	3600	0.04		• A process simulation study which assumed an electrolyser efficiency of 75 % (HHV basis). • Carbon in DRI is supplied by natural gas.
Biochar DRI	[13,62]	Lab scale data	6845					• A DRI process using solid biomass/biochar in a rotary hearth furnace. • The fuel energy demand is estimated based on the biochar consumption of 0.80 t/*t*-DRI [13] and biochar LHV of 30.8 MJ/kg [66].

[a] CO_2 is ready for transport and storage at 15 bar, −28 °C.

[b] Concentrated CO_2 stream (100 vol%) at 1 bar, 230 °C.

consumption (>65 %) is mainly due to the required additional heat for the MEA reboiler unit, which is assumed to be provided by an electric boiler in this study. In detail, the presented biosyngas DRI route has a specific energy demand of CO_2 capture between 880 and 1060 kWh/t-DRI, at least 40 % of which is provided through heat recovery. This result is comparable with the study of Arasto et al. [65], which presented a technical concept analysis of an MEA-based post-combustion CO_2 capture method at a Nordic blast furnace (Raahe steel plant, Finland). The study found that, for each t produced hot metal (HM), a specific energy demand of 770–1100 kWh is required for capturing 0.77–1.15 t CO_2 from the blast furnace gas.

The energy consumption of the CO_2 capture unit could be lowered through advanced heat integration of low-temperature waste heat streams and the adjustment of the CO_2 capture operating parameters. For instance, Arasto et al. [65] suggest using a low-temperature solvent, rather than MEA, to capture a higher amount of CO_2 owing to the higher ability to utilise low exergy heat. The same study also demonstrates the possibility of heating the solvent reboiler unit by recovering the waste heat streams from the steelmaking part of an integrated steel mill. Thus, the possibility of using other heat sources from downstream processes should also be considered in the real application. Other low-temperature heat recovery technologies, such as heat pumps, can also be considered for heating the solvent reboiler unit [58]. Furthermore, new-generation chemical absorbents are currently being developed and tested at pilot scales, which potentially have a lower energy demand in terms of reboiler duties. As summarised by Bui et al. [46], some examples of these new absorbents are blended MEA with methyldiethanolamine (MEA/MDEA), aqueous blended piperazine/2-amino-2-methyl-1-propanol (PZ/AMP), ammonia (NH_3), and potassium carbonate (K_2CO_3), which may have approximately 15–43 % lower reboiler duty than that of 30 wt % MEA. Nevertheless, very rare information is currently available on the commercial applications of these new-generation absorbents.

4. Conclusion

This work proposes a biosyngas DRI production system to produce hot DRI with 92 % degrees of metallisation and 2 % carbon content. The system was modelled and evaluated by using the Aspen Plus V12 software package. Several integration scenarios are proposed based on gasifier types and tar reformer heat sources. The scenarios consist of two main categories: steam-blown DFB-based and steam/oxygen-blown CFB-based scenarios. Different integration scenarios are proposed for each main category based on applying an integrated biomass dryer, ASU, electrolyser, or electrified tar reformer.

The results of this study can be summarised as follows.

- The proposed biomass gasification and subsequent syngas conditioning and cleaning process could produce a reducing gas with an RP value range between 12.6 and 111.8, which meets the minimum requirement of the existing gas-based DRI shaft furnace (RP ratio > 9).
- The gross energy demand for steam/oxygen-blown CFB scenarios is generally higher than the steam DFB scenarios due to the higher electricity demand for CO_2 capture and liquefaction. The captured CO_2 ranges between 0.65 and 0.91 and 0.77–1.13 t/t-DRI for the case of steam DFB and steam/oxygen CFB scenarios, respectively.
- Among the scenarios that use autothermal tar reformers, the application of electrolyser to provide O_2 and additional H_2 results in the highest gross energy demand, owing to its highest electricity demand. In contrast, the electrification of the tar reformer and the gas heater has the lowest gross energy demand than other integration scenarios, with a relatively lower electricity demand than that of electrolyser scenarios. In addition, electrification of the tar reformer and gas heater reduces the generated and captured CO_2 by approximately 29–32 %.

- An integrated biomass dryer heated by the combustion of excess top gas is proven to handle the high moisture content feedstock without sacrificing the system's overall energy efficiency.
- Regarding energy demand, the proposed biosyngas DRI route has comparable performance to other DRI routes, such as the well-established natural gas and coal gasification DRI routes. In addition, the estimated net energy demand of the investigated systems can be at least ~ 22 % lower than that of gross value, which indicates an even more competitive performance if optimisation of the process can be developed properly.

The present study has mainly focused on evaluating the different process configuration of the syngas production and conditioning; thus, more work on developing process configuration and sensitivity analysis of the DRI furnace itself are demanded for future works. These works may include the technical analysis of different DRI furnaces (e.g., fluidised bed furnaces) and iron ore agglomerates/concentrates. More importantly, attention should be given to identifying a suitable process configuration from a technical, operational and economic point of view.

CRediT authorship contribution statement

Ilman Nuran Zaini: Conceptualization, Methodology, Investigation, Formal analysis, Visualization, Writing – original draft, Writing – review & editing. **Anissa Nurdiawati:** Investigation, Writing – original draft, Writing – review & editing. **Joel Gustavsson:** Methodology, Writing – review & editing. **Wenjing Wei:** Methodology, Writing – review & editing. **Henrik Thunman:** Conceptualization, Writing – review & editing. **Rutger Gyllenram:** Conceptualization, Project administration, Writing – review & editing, Funding acquisition. **Peter Samuelsson:** Conceptualization, Project administration, Writing – review & editing, Funding acquisition. **Weihong Yang:** Conceptualization, Writing – review & editing.

Declaration of Competing Interest

The authors declare that they have no known competing financial interests or personal relationships that could have appeared to influence the work reported in this paper.

Data availability

Data will be made available on request.

Acknowledgements

Appendix A. Supplementary material

Supplementary data to this article can be found online at https://doi.org/10.1016/j.enconman.2023.116806.

References

[1] IEA. Iron and Steel Technology Roadmap. Paris, France; 2020. doi: 10.1787/3dcc2a1b-en.
[2] Nurdiawati A, Urban F. Towards deep decarbonisation of energy-intensive industries: a review of current status. Technol Policies Energies 2021;14:2408. https://doi.org/10.3390/en14092408.
[3] Somers J. Technologies to decarbonise the EU steel industry, EUR 30982 EN, Publications Office of the European Union, Luxembourg. Luxembourg 2022. https://doi.org/10.2760/069150.
[4] Mousa E, Wang C, Riesbeck J, Larsson M. Biomass applications in iron and steel industry: an overview of challenges and opportunities. Renew Sustain Energy Rev 2016;65:1247–66. https://doi.org/10.1016/j.rser.2016.07.061.

[5] Zaini IN, Sophonrat N, Sjöblom K, Yang W. Creating values from biomass pyrolysis in Sweden: co-production of H2. Biocarbon Bio-Oil Processes 2021;9:1–21.

[6] Swedish Energy Agency. State aid for BECCS 2022. Available from: http://www.energimyndigheten.se/en/sustainability/carbon-capture-and-storage/state-aid-for-beccs/ (accessed September 28, 2022).

[7] Nurdiawati A, Urban F. Decarbonising the refinery sector: a socio-technical analysis of advanced biofuels, green hydrogen and carbon capture and storage developments in Sweden. Energy Res Soc Sci 2022;84:102358. https://doi.org/10.1016/j.erss.2021.102358.

[8] Mousa E, Wang C, Riesbeck J, Larsson M. Biomass applications in iron and steel industry: an overview of challenges and opportunities. Renew Sustain Energy Rev 2016;65:1247–66. https://doi.org/10.1016/j.rser.2016.07.061.

[9] Wei R, Zhang L, Cang D, Li J, Li X, Xu CC. Current status and potential of biomass utilization in ferrous metallurgical industry. Renew Sustain Energy Rev 2017;68: 511–24. https://doi.org/10.1016/j.rser.2016.10.013.

[10] Suopajärvi H, Kemppainen A, Haapakangas J, Fabritius T. Extensive review of the opportunities to use biomass-based fuels in iron and steelmaking processes. J Clean Prod 2017;148:709–34. https://doi.org/10.1016/j.jclepro.2017.02.029.

[11] Suopajärvi H, Pongrácz E, Fabritius T. Bioreducer use in Finnish blast furnace ironmaking – analysis of CO2 emission reduction potential and mitigation cost. Appl Energy 2014;124:82–93. https://doi.org/10.1016/j.apenergy.2014.03.008.

[12] Suopajärvi H, Fabritius T. Towards more sustainable ironmaking—an analysis of energy wood availability in Finland and the economics of charcoal production. Sustainability 2013;5:1188–207. https://doi.org/10.3390/su5031188.

[13] Han H, Duan D, Yuan P, Li D. Biomass reducing agent utilisation in rotary hearth furnace process for DRI production. Ironmak Steelmak 2015;42:579–84. https://doi.org/10.1179/1743281215Y.0000000001.

[14] Suman S, Yadav AM. Biomass Derived Carbon for the Reduction of Iron Ore Pellets. In: Pal S, Roy D, Sinha SK, editors. Process. Charact. Mater., vol. 13, Springer Singapore; 2021, p. 369–70. doi: 10.1007/978-981-16-3937-1.

[15] Midrex Technologies Inc. MIDREX NG: Optimizing DRI production using natural gas. 2018.

[16] Bolívar Caballero JJ, Zaini IN, Yang W. Reforming processes for syngas production: a mini-review on the current status, challenges, and prospects for biomass conversion to fuels. Appl Energy Combust Sci 2022;10:100064. https://doi.org/10.1016/j.jaecs.2022.100064.

[17] Molino A, Larocca V, Chianese S, Musmarra D. Biofuels production by biomass gasification: a review. Energies 2018;11:1–31. https://doi.org/10.3390/en11040811.

[18] Carvalho MM., Cardoso M, Vakkilainen EK. Bio-SNG production in Brazil : Applications in the iron and steel industry. In: Conf. 9th Japan-Brazil Symp. Dust Process. Metall. Ind.; 2013.

[19] Gunarathne DS, Mellin P, Yang W, Pettersson M, Ljunggren R. Performance of an effectively integrated biomass multi-stage gasification system and a steel industry heat treatment furnace. Appl Energy 2016;170:353–61. https://doi.org/10.1016/j.apenergy.2016.03.003.

[20] Nwachukwu CM, Toffolo A, Wetterlund E. Biomass-based gas use in Swedish iron and steel industry – Supply chain and process integration considerations. Renew Energy 2020;146:2797–811. https://doi.org/10.1016/j.renene.2019.08.100.

[21] Grip CE, Toffolo A, Östman M, Sandbergdand E, Orre J. Forestry meets Steel. A system study of the possibility to produce DRI (directely Reduced Iron) using gasified biomass. In: ECOS 2015 - 28th Int. Conf. Effic. Cost, Optim. Simul. Environ. Impact Energy Syst.; 2015. p. 1–12.

[22] Pissot S, Thunman H, Samuelsson P, Seemann M. Production of negative-emissions steel using a reducing gas derived from DFB gasification. Energies 2021;14:4835. https://doi.org/10.3390/en14164835.

[23] Hedayati A, Soleimanisalim AH, Mattisson T, Lyngfelt A. Thermochemical conversion of biomass volatiles via chemical looping: comparison of ilmenite and steel converter waste materials as oxygen carriers. Fuel 2022;313:122638. https://doi.org/10.1016/j.fuel.2021.122638.

[24] Li XT, Grace JR, Lim CJ, Watkinson AP, Chen HP, Kim JR. Biomass gasification in a circulating fluidized bed. Biomass Bioenergy 2004;26:171–93. https://doi.org/10.1016/S0961-9534(03)00084-9.

[25] Pio D, Tarelho LAC. Industrial gasification systems (>3 MWth) for bioenergy in Europe: current status and future perspectives. Renew Sustain Energy Rev 2021; 145:111108. https://doi.org/10.1016/j.rser.2021.111108.

[26] Gong Y, Wang X, Chen D, Al-Qadri BMH. Retrospect and prospect of carbon stripper technology in solid-fuel chemical looping combustion. Fuel Process Technol 2021;221:106920. https://doi.org/10.1016/j.fuproc.2021.106920.

[27] MIDREX. Direct from MIDREX 2019. Available from: https://www.midrex.com/wp-content/uploads/Midrex_2019_DFM3QTR_Final.pdf (accessed March 21, 2022).

[28] Swedish Bioenergy Assn (Svebio). Roadmap Bioenergy – meeting the demand for bioenergy in a fossil free Sweden 2020.

[29] Skogsstyrelsen. Skogliga konsekvensanalyser 2022 - virkesbalanser (Forestry Impact Assessments 2022 - Timber Balances). 2022 (Sweden).

[30] Aspentech. Aspen Plus® n.d. Available from: https://www.aspentech.com/en/products/engineering/aspen-plus (accessed October 11, 2022).

[31] Alamia A, Larsson A, Breitholtz C, Thunman H. Performance of large-scale biomass gasifiers in a biorefinery, a state-of-the-art reference. Int J Energy Res 2017;41: 2001–19. https://doi.org/10.1002/er.3758.

[32] Arzpeyma N, Gyllenram R. RAWMATMIX® Standard materials and energy sources 20210110. Kobolde Partners AB n.d. doi: 10.13140/RG.2.2.32940.69760.

[33] Alamia A, Ström H, Thunman H. Design of an integrated dryer and conveyor belt for woody biofuels. Biomass Bioenergy 2015;77:92–109. https://doi.org/10.1016/j.biombioe.2015.03.022.

[34] Wan W, Engvall K, Yang W. Novel model for the release and condensation of inorganics for a pressurized fluidized-bed gasification process: effects of gasification temperature. ACS Omega 2018;3:6321–9. https://doi.org/10.1021/acsomega.8b00019.

[35] Hannula I, Kurkela E. A parametric modelling study for pressurised steam/O2-blown fluidised-bed gasification of wood with catalytic reforming. Biomass Bioenergy 2012;38:58–67. https://doi.org/10.1016/j.biombioe.2011.02.045.

[36] Zaini IN, Nurdiawati A, Aziz M. Cogeneration of power and H2 by steam gasification and syngas chemical looping of macroalgae. Appl Energy 2017;207: 134–45. https://doi.org/10.1016/j.apenergy.2017.06.071.

[37] Channiwala SA, Parikh PP. A unified correlation for estimating HHV of solid, liquid and gaseous fuels. Fuel 2002;81:1051–63. https://doi.org/10.1016/S0016-2361(01)00131-4.

[38] Pissot S, Faust R, Aonsamang P, Berdugo Vilches T, Maric J, Thunman H, et al. Development of oxygen transport properties by olivine and feldspar in industrial-scale dual fluidized bed gasification of woody biomass. Energy Fuel 2021;35(11): 9424–36.

[39] Larsson A, Kuba M, Berdugo Vilches T, Seemann M, Hofbauer H, Thunman H. Steam gasification of biomass – typical gas quality and operational strategies derived from industrial-scale plants. Fuel Process Technol 2021;212:106609. https://doi.org/10.1016/j.fuproc.2020.106609.

[40] Alamia A, Òsk Gardarsdòttir S, Larsson A, Normann F, Thunman H. Efficiency comparison of large-scale standalone, centralized, and distributed thermochemical biorefineries. Energy Technol 2017;5:1435–48. https://doi.org/10.1002/ente.201600719.

[41] Thunman H, Seemann M, Berdugo Vilches T, Maric J, Pallares D, Ström H, et al. Advanced biofuel production via gasification - lessons learned from 200 man-years of research activity with Chalmers' research gasifier and the GoBiGas demonstration plant. Energy Sci Eng 2018;6(1):6–34.

[42] Wen Y, Wang S, Shi Z, Nuran Zaini I, Niedzwiecki L, Aragon-Briceno C, et al. H2-rich syngas production from pyrolysis of agricultural waste digestate coupled with the hydrothermal carbonization process. Energy Convers Manag 2022;269:116101. https://doi.org/10.1016/j.enconman.2022.116101.

[43] Wang S, Wen Y, Shi Z, Nuran Zaini I, Göran Jönsson P, Yang W. Novel carbon-negative methane production via integrating anaerobic digestion and pyrolysis of organic fraction of municipal solid waste. Energy Convers Manag 2022;252: 115042. https://doi.org/10.1016/j.enconman.2021.115042.

[44] Voss B, Madsen J, Hansen JB, Andersson KJ. Topsøe Tar Reforming in Skive - the tough get going. Catal Rev 2016.

[45] Andersson KJ, Skov-Skjøth Rasmussen M, Højlund Nielsen PE. Industrial-scale gas conditioning including Topsoe tar reforming and purification downstream biomass gasifiers: an overview and recent examples. Fuel 2017;203:1026–30. https://doi.org/10.1016/j.fuel.2017.02.085.

[46] Bui M, Adjiman CS, Bardow A, Anthony EJ, Boston A, Brown S, et al. Carbon capture and storage (CCS): the way forward. Energy Environ Sci 2018;11(5): 1062–176.

[47] Xu ZY, Wang RZ, Yang C. Perspectives for low-temperature waste heat recovery. Energy 2019;176:1037–43. https://doi.org/10.1016/j.energy.2019.04.001.

[48] Seo Y, Huh C, Lee S, Chang D. Comparison of CO 2 liquefaction pressures for ship-based carbon capture and storage (CCS) chain. Int J Greenh Gas Control 2016;52: 1–12. https://doi.org/10.1016/j.ijggc.2016.06.011.

[49] Ministry of Petroleum and Energy. Feasibility study for full-scale CCS in Norway 2016.

[50] Béchara R, Hamadeh H, Mirgaux O, Patisson F. Carbon impact mitigation of the iron ore direct reduction process through computer-aided optimization and design changes. Metals (Basel) 2020;10:367. https://doi.org/10.3390/met10030367.

[51] Hamadeh H, Mirgaux O, Patisson F. Detailed modeling of the direct reduction of iron ore in a shaft furnace. Materials (Basel) 2018;11:1865. https://doi.org/10.3390/ma11101865.

[52] Stephenson RL, Smailer RM. Direct reduced iron: technology and economics of production and use. United States; 1980.

[53] Jess A, Depner H. Reduction and carburization of iron-ore in a fluidized bed by CO, H2 and CH4. Steel Res 1998;69:77–84. https://doi.org/10.1002/srin.199801454.

[54] Cheeley R, Leu M. Coal gasification for DRI production - an Indian solution. Steel Times Int 2010.

[55] Niu M, Xie J, Liang S, Liu L, Wang L, Peng Y. Simulation of a new biomass integrated gasification combined cycle (BIGCC) power generation system using Aspen Plus: performance analysis and energetic assessment. Int J Hydrogen Energy 2021;46:22356–67. https://doi.org/10.1016/j.ijhydene.2021.04.076.

[56] Pfaff I, Kather A. Comparative thermodynamic analysis and integration issues of CCS steam power plants based on oxy-combustion with cryogenic or membrane based air separation. Energy Procedia 2009;1:495–502. https://doi.org/10.1016/j.egypro.2009.01.066.

[57] Rechberger K, Spanlang A, Sasiain Conde A, Wolfmeir H, Harris C. Green hydrogen-based direct reduction for low-carbon steelmaking. Steel Res Int 2020; 91:2000110. https://doi.org/10.1002/srin.202000110.

[58] Andersson V, P-ÿke F, Berntsson T. Techno-economic analysis of excess heat driven post-combustion CCS at an oil refinery. Int J Greenh Gas Control 2016;45:130–8. https://doi.org/10.1016/j.ijggc.2015.12.019.

[59] Arasto A, Tsupari E, Kärki J, Lilja J, Sihvonen M. Oxygen blast furnace with CO 2 capture and storage at an integrated steel mill—Part I: Technical concept analysis. Int J Greenh Gas Control 2014;30:140–7. https://doi.org/10.1016/j.ijggc.2014.09.004.

[60] Technologies LG. Ironmaking process alternative screening study Vl. I. US Dep Energy 2000.

[61] Pardo N, Moya JA, Vatopoulos K. Prospective scenarios on energy efficiency and CO2 emissions in the EU iron & steel industry. JRC Sci Policy Report, JRC74811 2012.

[62] Fan Z, Friedmann SJ. Low-carbon production of iron and steel: Technology options, economic assessment, and policy. Joule 2021;5:829–62. https://doi.org/10.1016/j.joule.2021.02.018.

[63] Echterhof T. Review on the use of alternative carbon sources in EAF steelmaking. Metals (Basel) 2021;11:222. https://doi.org/10.3390/met11020222.

[64] Hornby S, Brooks G. Impact of hydrogen DRI on EAF steelmaking. Direct from MIDREX 2021. Available from: https://www.midrex.com/tech-article/impact-of-hydrogen-dri-on-eaf-steelmaking/ (accessed November 14, 2022).

[65] Arasto A, Tsupari E, Kärki J, Pisilä E, Sorsamäki L. Post-combustion capture of CO2 at an integrated steel mill – Part I: Technical concept analysis. Int J Greenh Gas Control 2013;16:271–7. https://doi.org/10.1016/j.ijggc.2012.08.018.

[66] Zhang Y, Ma Z, Zhang Q, Wang J, Ma Q, Yang Y, et al. Comparison of the physicochemical characteristics of bio-char pyrolyzed from moso bamboo and rice husk with different pyrolysis temperatures. BioResources 2017;12(3).